Review

International Journal of Modern Physics B
Vol. 20, No. 7 (2006) 747–778

World Scientific
www.worldscientific.com

NOVEL LIQUID CRYSTALLINE PHASES IN QUANTUM HALL SYSTEMS

CARLOS WEXLER

Department of Physics and Astronomy, University of Missouri, Columbia, Missouri 65211, USA

ORION CIFTJA

Department of Physics, Prairie View A&M University, Prairie View, Texas 77446, USA

Received 26 January 2006

Since 1999, experiments have shown a plethora of surprising results in the low-temperature magnetotransport in intermediate regions between quantum Hall (QH) plateaus: the extreme anisotropies observed for half-filling, or the re-entrant integer QH effects at quarter filling of high Landau levels (LL); or even an apparent melting of a Wigner Crystal (WC) at filling factor $\nu = 1/7$ of the lowest LL. A large body of seemingly distinct experimental evidence has been successfully interpreted in terms of liquid crystalline phases in the two-dimensional electron system (2DES). In this paper, we present a review of the physics of liquid crystalline states for strongly correlated two-dimensional electronic systems in the QH regime. We describe a semi-quantitative theory for the formation of QH smectics (stripes), their zero-temperature melting onto nematic phases and ultimate anisotropic-isotropic transition via the Kosterlitz–Thouless (KT) mechanism. We also describe theories for QH-like states with various liquid crystalline orders and their excitation spectrum. We argue that resulting picture of liquid crystalline states in partially filled LL-s is a valuable starting point to understand the present experimental findings, and to suggest new experiments that will lead to further elucidation of this intriguing system.

Keywords: Two-dimensional electronic system; quantum Hall effects; liquid crystals; topological phase transitions.

1. Introduction

Strongly correlated two-dimensional electron systems (2DES) subject to a high perpendicular magnetic field have been providing various fascinating phenomena for more than 25 years. In particular, the observation of the integer quantum Hall (QH) effect (IQHE)[1] and of the fractional QH effect (FQHE)[2,3] are some of the most remarkable phenomena of the 20th century, rivaling that of superfluidity and superconductivity in their macroscopic manifestation of quantum mechanical effects. This has caused a tremendous impetus on the development of many novel ideas in many-body physics,[4,5] like the existence of fractionally charged quasiparticles,[3]

topological quantum numbers,[6] chiral Luttinger liquids,[7,8] composite particles,[a,9] etc. One of the reasons that 2DES keep supplying novel and exciting results is the improved quality of the samples with mobilities increasing roughly exponentially with time, thus allowing the emergence of new, subtler effects due to electronic correlations (which are enhanced because of the reduced dimensionality, and because the strong perpendicular magnetic field quenches the kinetic energy into Landau levels–LL).

There are notable experimental similarities between the IQHE and FQHE, however, the physical interpretation is quite different: the former is due essentially to "one-body" physics (a mere, albeit non-trivial, consequence of LL quantization and localization by disorder[4,5]); the latter stands out as pure quantum many-body phenomena which results from the condensation of strongly correlated electrons into an incompressible isotropic liquid state formed at special electronic densities of the 2DES (Jain's composite fermion theory — CF[9] (see also footnote a), however, gives a unified understanding of both phenomena).

In the lowest Landau level (LLL) things are relatively well understood even though the electronic phase diagram for filling factors $0 < \nu \leq 1$ where all electrons are fully spin polarized is quite intricate with various competing phases. It is believed that for filling factors ν smaller than a critical value $\nu_c \approx 6.5$ Wigner crystallization (WC) occurs[10–14] (note, however, that for $\nu = 1/7 < \nu_c$, melting of the WC into a FQHE-like state appears to have been observed,[15] this will be discussed in later sections), while condensation of electrons into an *incompressible isotropic FQHE liquid* state occurs at filling factors, $\nu = 1/3, 2/5, 3/7, \ldots$ and $\nu = 1/5, 2/9, \ldots$ The principal sequences of the FQHE liquid states who originate from $\nu = 1/3$ and $1/5$, namely filling factors of the form: $\nu = p/(2mp \pm 1)$, where p, m are integers, is thoroughly understood in terms of Laughlin's ingenious wavefunction[3] and the elegant composite fermion (CF) theory[9] (see also footnote a). A special place is reserved for the half filled state, $\nu = 1/2$ which is believed to be a *compressible isotropic Fermi liquid* state[16–18] different from the other incompressible FQHE liquid states of the originating sequence. The Halperin–Lee–Read (HLR) theory[19] shed light on the Fermi-liquid nature of the LLL $\nu = 1/2$ state (Landau level index $L = 0$) which is now believed to be a compressible CF Fermi liquid state with a well-defined isotropic Fermi surface. Differently from other LLL odd denominator filled states, the LLL half-filled state does not show the typical FQHE features and typically behaves as a metallic state. Similar (but more complex) behavior is observed for $1 < \nu \leq 2$, i.e. for the upper spin sub-band of the LLL.

The situation is dramatically different for higher filling factors, $2 < \nu \leq 4$ (electrons in the first excited LL with index $L = 1$) and $4 < \nu \leq 6$ (electrons in the

[a]For a review, see J. Jain, The composite fermion: a quantum particle and its quantum fluids, *Physics Today*, Apr/2000, p. 39; and/or *Composite Fermions*, ed. O. Heinonen (World Scientific, New York, 1998).

second excited LL with index $L = 2$). For $L = 1$, the FQHE is almost absent with the exception of the exotic $\nu = 5/2$ state which shows a *quantized* (though weak) Hall conductance observed along with a strong reduction of the longitudinal conductance[20,21] which indicates a possible pairing instability of the CF-s.[22–28] A discussion of the $\nu = 5/2$ state which is the only known even-denominator FQHE state is a complex topic by itself and, along with the properties of the $\nu = 3/2$ and $7/2$ states (half filling of the upper spin sub-band) will not be discussed here. Current experimental evidence indicates that for $L = 1$ electronic states are isotropic, and thus outside the scope of this paper. Closer to the topic of this paper, however, is what is seen in higher LL-s ($L \geq 2$), where early theoretical approaches had suggested the presence of intriguing charge density waves (CDW).[29–31] Remarkably, these basic approaches were confirmed, in part, by some of the most remarkable experimental findings of the recent years: the discovery of extreme magnetotransport anisotropy in the longitudinal resistivities around half-filled upper LL-s with indices $L \geq 2$ corresponding to filling factors $\nu = 9/2, 11/2$, etc.[32–36] To complete the picture at high LL-s, additional phases have been observed, such as the reentrant IQHE states at close to quarter-filling of high LL-s, and other insulating phases.[37–39]

In this paper we will discuss some aspects of the theoretical understanding that has emerged over the past few years towards understanding these complex and seemingly diverse phenomena. In Sec. 2 we will expand on the experimental evidence available that support a liquid-crystalline picture. Section 3 describes early theoretical approaches based on CDW-s, which generally suffered from overestimating the formation energy of such structures. Section 4 discusses how to reconcile the early theories with experiments, involving excitations and topological defects of the C'S-s, and ultimately producing a semi-quantitative agreement with experimental values of the anisotropic-isotropic transition temperatures. In Sec. 5, broken rotational symmetry (BRS) states are proposed to generate various anisotropic phases at the quantum level. A description of the collective excitations of the BRS states is then proposed in Sec. 6, based on the single mode approximation (SMA). Finally, Sec. 7 presents a summary of this paper, highlighting the accomplishments of the liquid crystalline perspective, and its current limitations.

2. Experimental Evidence

2.1. *Anisotropic phases*

Recent transport experiments in very high mobility ($\mu \sim 10^7$ m/Vs) $GaAs/Al_xGa_{1-x}As$ heterostructures[32–36] established a qualitative difference between the half filled states at higher Landau levels with index $L = 2, 3, \ldots$ and those in the LLL ($L = 0$) and first excited Landau level ($L = 1$). These experiments revealed the existence of regimes of magnetic fields which correspond to filling factors around $\nu = 9/2, 11/2, 13/2$, etc. in which the 2DES exhibits characteristics of a compressible liquid with an unexpectedly large temperature-dependent

anisotropy in its magnetotransport properties. The effect is strongest in the second excited LL with index $L = 2$ around filling factors $\nu = 9/2$ and $\nu = 11/2$ but persist up to about $L = 6$. The attenuation of the anisotropy with increasing filling factor (as L increases) is generally monotonic, but contains a noticeable oscillatory dependence upon the spin sub-level. Such highly anisotropic states with strong anisotropic longitudinal resistance develop at a temperature only below about 150 mK near half-filling of highly excited LL-s. Even though the effect is more pronounced at half-filling of higher LL-s it remains substantial in a range of filling factors, $\Delta\nu \approx 0.2$ around this state.

For current flow in one direction, the longitudinal resistance exhibits a strong maximum while in the transverse direction a minimum occurs. In all high-mobility GaAs samples the "easy" transport direction is roughly along $\langle 110 \rangle$ and the "hard" transport direction is along $\langle 1\bar{1}0 \rangle$ where $\langle 110 \rangle$ and $\langle 1\bar{1}0 \rangle$ are the natural cleavage directions in GaAs. When the current is flown along the $\langle 1\bar{1}0 \rangle$ (hard axis) the longitudinal resistance in several orders of magnitude larger than the longitudinal resistance measured for the case of a current flown along $\langle 1\bar{1}0 \rangle$ direction (easy axis).[b] Equally striking is the fact that no comparable anisotropy is seen for the $L = 1$ Landau level (filling factors $\nu = 5/2$ or $\nu = 7/2$) and the $L = 0$ Landau level.

The main experimental findings are as follows:

(i) The magnetotransport anomalies are observed in clean high mobility 2DES in GaAs/AlGaAs samples, but no anisotropy has been reported in lower mobility samples which show instead conventional phase transitions between quantum Hall states.

(ii) The effects abruptly begin only below about ca. 150 mK, and are strongest in the second excited Landau level ($L = 2$), but persist up to LL-s as high as $L = 6$.

(iii) No comparable anisotropy is apparent in the LLL ($L = 0$), nor the the first excited Landau level ($L = 1$).

(iv) As the temperature is lowered below ca. 50 mK, the longitudinal resistance grows very rapidly, while the transverse (Hall) resistance becomes smaller. The ratio of the two approaches a constant between two and three orders of magnitude (see also footnote b).

(v) The reported anisotropy is apparently confined to the centers of the LL-s around the half filled state.

(vi) For no current configuration are any plateaus seen in the Hall resistance at half filling of the Landau levels with index $L = 2, 3, \ldots$

(vii) The orientation of anisotropy is fixed within the sample (but can be reoriented by the application of an in-plane magnetic field).

(viii) The onset of anisotropy is keyed to the filling factor and not the magnetic field itself.

[b]The effect is exaggerated by the current distribution geometry; the intrinsic anisotropy is smaller: $\rho_{xx}/\rho_{yy} \sim 20$. See S. Simon, *Phys. Rev. Lett.* **83**, 4223 (1999).

(ix) The anisotropy gradually disappears in the semiclassical regime at very low magnetic fields.

2.2. *Other possible liquid crystalline phases*

In the realms of FQHE, one of the oldest questions concerns the transition point between the series of FQHE states and the Wigner crystal (WC).[3–5,10–14,40] Initial estimations by Laughlin predicted the transition at $\nu_c \simeq 1/10$,[3] with subsequent improvements leading to an estimate of $\nu_c \simeq 1/6.5$[10] or even at higher filling factors.[4,5,14] The structure of the WC corresponds to a hexagonal lattice.

Recently, for very high mobility GaAs/Al_xGa_{1-x}As heterostructures, Pan *et al.*[15] have discovered evidence that for a window of temperatures above a filling-factor-specific temperature (e.g. ca. 135 mK for $\nu = 1/7$) an apparent fractional QHE (FQHE) is observed, as evidenced by a dip in the longitudinal resistance for various *very low* filling factors such as $\nu = 2/11$, 3/17, 3/19, 2/13, 1/7, 2/15, 2/17 and 1/9, corresponding to the hierarchical sequences of composite fermion (CF) states that originate from the $\nu = 1/6$ and $\nu = 1/8$ "Fermi seas" (see also footnote a) (and which correspond to attaching six and eight vortices to each electron, respectively). These recent experimental findings of an apparent FQHE state at finite temperatures corroborate earlier measurements showing a re-entrant behavior at $\nu = 1/7$ and 2/9,[41,42] although these features disappear as $T \to 0$. The general consensus is that the "true" ground state is, indeed, the WC and that the observations correspond of *melting* of such WC toward a correlated liquid state such as the FQHE's.

This explanation has shortcomings, however. Since the WC is the lowest *energy* state and has a gapless excitation spectrum (for neutral excitations), it is difficult to see how the *free energy* $A = E - TS$ for the Laughlin state can be lower at finite temperatures, especially because the latter is gaped and hence should have lower entropy S, at least at very low temperatures. More refined arguments, which consider the entropy of the Laughlin state at temperatures high enough that there is a significant number of excitations across the gap, have shown that the FQHE state entropy may raise rapidly,[43,44] which could explain the possibility of this WC to FQHE melting transition. The calculated transition temperature for the $\nu = 1/7$ state should be 400–600 mK,[43,44] considerably higher than the experimental result of ∼135 mK[15] (the difference is not necessarily unsatisfactory given the nature of the approximations needed for the calculation).

3. Early Theoretical Work: Charge Density Waves

Although the fundamental origin of the anisotropy is still unknown, a unidirectional charge density wave (UCDW) is a plausible candidate for the anisotropic state. Earlier theoretical work[29–31] had shown that a 2DES can have a UCDW ground state in weak magnetic fields (for nearly half-filling of high LL-s, see Fig. 1). This theoretical work was based on the Hartree–Fock (HF) approximation and

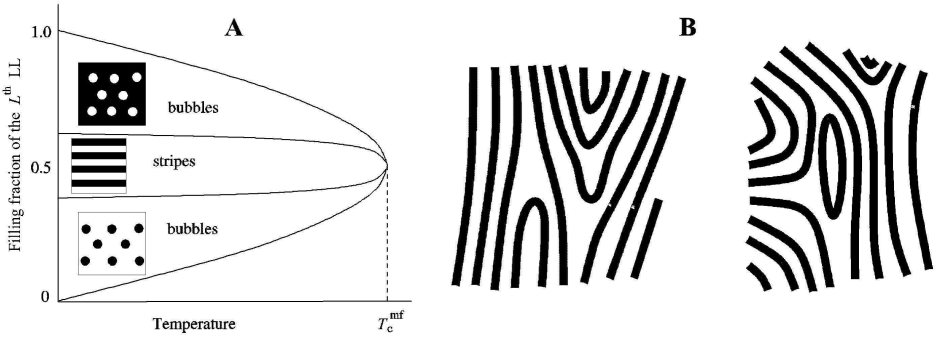

Fig. 1. Panel A: Basic phase diagram for a partially-filled LL. Note the presence of stripped and bubble phases. The stripes are assumed to be at the core of the anisotropies observed in magnetotransport. Panel B: An improvement over the static stripes model: vibrations (phonons) and topological defects (dislocations, disclinations) reduce the stripe order to that of a *nematic*, eventually rendering the system isotropic via the Kosterlitz–Thouless disclination unbinding mechanism.

the main conclusion is that electrons in the partially occupied L-th Landau level form domains (stripes) with filling factors equal to 1 and 0 that alternate with a spatial period of the order of the cyclotron radius. A UCDW corresponds to a state with broken rotational symmetry and density modulation therefore it can be viewed as a quantum Hall *smectic* (QHS) state. For instance, at filling factor $\nu = 9/2$, which corresponds to half filling of the lower spin branch of the $L = 2$ Landau level, the UCDW would consist of filled stripes alternated by empty ones. The HF-based UCDW theory implies that stripes should form at a temperature in the order of few Kelvins (see Fig. 2).[29–31,45–47] Such a high critical temperature contrasts with the experimental observation that anisotropy only sets in at much lower temperatures of the order of 100–150 mK.[32–36] Even though factors not included in the HF approximation of the UCDW theory may account for some of the discrepancies with the experiment, other scenarios are plausible.

An alternative approach that would be consistent with the observed experimental anisotropy would view the onset of such anisotropy as signature of a phase transition from an isotropic to an anisotropic phase. Fradkin and Kivelson[45,46] suggested that the appearance of the anisotropy reflects the orientational ordering of local regions having a pre-existing order, in analogy with what happens in an isotropic-to-nematic liquid transition. The onset of anisotropy is therefore viewed as a transition to a quantum Hall nematic (QHN) state, rather than the first signal of the creation of a UCDW modulation. They further argued that the inclusion of quantum and thermal fluctuations above the HF UCDW state leads to a variety of electronic crystalline states including a QHN phase which is stable at temperatures $T > 0$. Monte-Carlo (MC) simulation results[48] based on a model of a classical nematic in a symmetry breaking field appear to support the view that

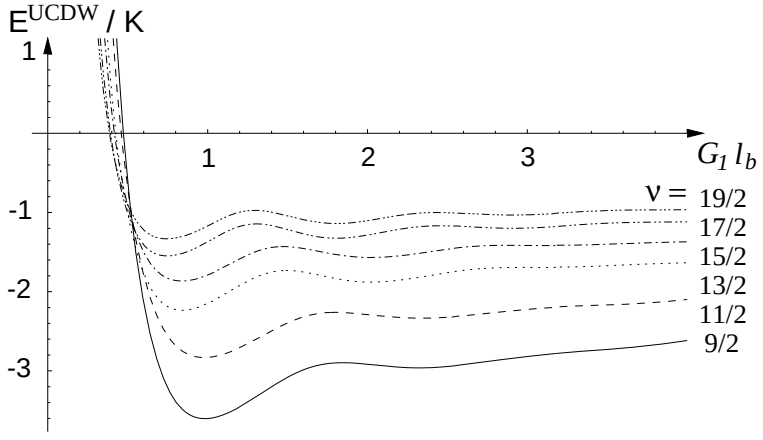

Fig. 2. Dependence of the average energy per electron state E^{UCDW} for various filling factors corresponding to anisotropic states. The calculations correspond to an electron density $n_e = 2.67 \times 10^1 1\ \mathrm{cm}^{-2}$, and a 2DES thickness $z_{\mathrm{rms}} = 58.3\,\text{Å}$.

anisotropic transport occurs when the 2DES is in a QHN phase (at least at finite temperature[c]).

Both smectic and nematic liquid crystalline states are natural candidates to explain the magnetotransport anisotropy observed in the experiments because both states break the rotational symmetry. However, as pointed out by Toner and Nelson,[49] the smectic always melts at any nonzero temperature, therefore, at least at finite temperatures, the nematic phase seems a slightly more plausible choice. On these grounds, one can interpret the transition to a nematic phase as a Kosterlitz-Thouless (KT) dislocation unbinding transition.[47,50–53] This idea will be covered in more detail in the next section. Alternatively, it is possible to formulate a "quantum Hall nematic" theory from scratch, without the need of the intermediate smectic phase. The latter approach will be further discussed in Sec. 5.

4. Smectics, Nematics and the Kosterlitz–Thouless Transition

4.1. *Hartree–Fock approximation for the CDW state*

To study the energetics of a CDW in the 2DES we follow the strategy developed by other authors,[54–56] and use the Hartree–Fock (HF) approximation, which corresponds to the assumption that the electronic state can be described as a Slater determinant of single-electron states. In the Landau gauge, $\mathbf{A}(\mathbf{r}) = (0, Bx, 0)$,

$$\psi_{\gamma\sigma n x_0}(\mathbf{r}) = \frac{\zeta_\gamma(z) e^{i x_0 y/l_b^2} H_n(\frac{x-x_0}{l_b}) e^{-(x-x_0)^2/2l_b^2}}{\pi^{1/4}(2^n n! L_y)^{1/2}}\,, \tag{1}$$

[c]At zero temperature, the existence of an ordered smectic phase is still unsettled. See A. H. MacDonald and M. P. A. Fisher, *Phys. Rev. B* **61**, 5724 (2000); H. Yi, H. A. Fertig and R. Côté, *Phys. Rev. Lett.* **85**, 4156 (2000).

where γ, σ, n and x_0 indicate the electric sub-band index (due to the confinement in the z direction), spin index, LL index, and guiding center; $l_b = (\hbar/eB)^{1/2}$ is the magnetic length, L_y is the length of the system in the y direction, and H_n are Hermite polynomials. Since the γ-splitting is very large, in what follows we consider only states with $\gamma = 0$: the system is *effectively two-dimensional*. We use these eigenstates as the basis for our calculations. In this basis the Coulomb interaction is modified by the presence of "structure factors" due to the density distribution:

$$M_{x_1,x_2}^{n_1,n_2}(\mathbf{q}) = \int d^3x e^{i\mathbf{q}\cdot\mathbf{r}} \psi^*_{0\sigma n_1 x_1}(\mathbf{r}) \psi_{0\sigma n_2 x_2}(\mathbf{r})\,. \tag{2}$$

These structure factors vanish for a discrete set of wavevectors thus eliminating the Coulomb repulsion for these wavevectors and facilitating the formation of a unidirectional CDW.[47] Since the anisotropic states occur for moderately weak magnetic fields where the level splitting between LL-s can be comparable to the interaction energies, we need to consider the polarizability of electrons in the lower (completely filled) LL-s, which can be computed in a straightforward way by means of the random phase approximation (RPA).[47,54–57] The reduction in the interaction strength allows for a great simplification: we only need to consider states within the valence LL, and in the absence of LL mixing, the state of the system is uniquely specified by the particle density function.[54–56,58] It is easy to see then that the energy of the system is a quadratic form in the density. In reciprocal space the energy per electron, relative to the uniform density case, can be written as[47]

$$E = \frac{1}{2\nu^*} \sum_j U(\mathbf{G}_j) |\Delta(\mathbf{G}_j)|^2\,, \tag{3}$$

where $\Delta(\mathbf{G}_j)$ is the Fourier coefficient of the occupation number at the reciprocal lattice vector $\mathbf{G}_j$ and the Coulomb kernel is $U(\mathbf{q}) = H(\mathbf{q}) - X(\mathbf{q})$, where H and X are the usual direct and exchange terms. The direct (repulsive) term dominates over small wavevectors (large distances) whereas the exchange (generally attractive) term dominates the large q region.

In the UCDW state, the occupation number of the valence LL alternates between 0 and 1 (see Fig. 3 and note that the actual electron density, ρ, has a considerably less dramatic oscillation due to the comparable sizes of the width of the wavefunctions and period of the UCDW), thus we have $\mathbf{G}_j = \mathbf{e}_x G_1 j$ with j an integer, and[47]

$$\Delta(\mathbf{G}_j) = \frac{\sin(\nu^* \pi j)}{\pi j}\,, \tag{4}$$

where $G_1 = 2\pi/a$, with a the period of the UCDW. Inserting this into Eq. (3) we find $E^{\mathrm{ucdw}}(G_1)$, the average energy per electron in the UCDW (see Fig. 2 and Table 1). The optimal UCDW corresponds to the minimum E^{ucdw}, and is observed at $a \simeq R_c \simeq 2.8 l_b \sqrt{2L+1}$).[29–31] In the optimal UCDW each electron gains one to a few degrees (see Table 1). Since the anisotropic-isotropic transition is observed at

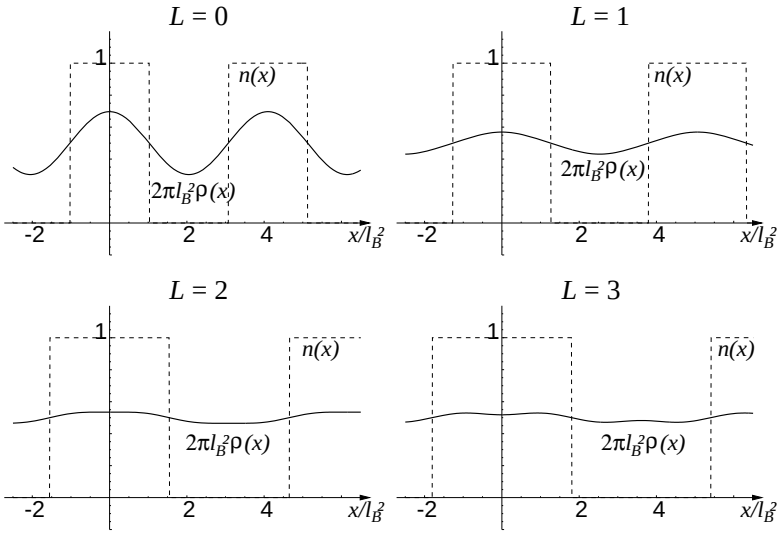

Fig. 3. Unidirectional CDW-s at the optimal period (which minimizes $E^{\rm ucdw}$, Fig. 2). Note that while the occupation number, n, oscillates as a "square wave" between 0 and 1, the actual electron density, ρ, has only a modest oscillation amplitude (for high L-s) due to the comparable sizes of the cyclotron radius, R_c, and the period of the UCDW, a.

Table 1. UCDW: Optimal wavevector G_1, period a, energy gain per electron $E^{\rm ucdw}$ and elastic constants B and K. The calculations were performed for the realization of Refs. 32–35.

ν	B(T)	l_b (Å)	$G_1 l_b$	a (Å)	$E^{\rm ucdw}$ (K)	$B(\mu{\rm K}/{\rm Å}^2)$	K(mK)
9/2	2.46	164	0.983	1048	−3.603	25.5	189
11/2	2.02	181	0.978	1163	−2.830	15.7	144
13/2	1.70	197	0.842	1470	−2.234	13.0	192
15/2	1.48	211	0.839	1580	−1.864	9.07	158
17/2	1.30	225	0.746	1895	−1.549	7.58	196
19/2	1.16	239	0.744	2018	−1.332	5.66	167

temperatures much smaller than this (ca. 100–150 mK), it should be clear that the observed transition cannot be related to the *formation* of the stripes, but rather, as we shall see, to the *unbinding of topological defects* in the existing stripes, as early suggested by Fradkin and Kivelson.[45–47]

4.2. *Low-energy excitations of the UCDW*

As we have seen above, the formation of the stripes is energetically favorable due to the competition between direct and exchange terms. Therefore, it is evident that the stripes should be formed at temperatures comparable to these energy gains (a few K). The presence of such stripes would clearly have profound effects on the magnetotransport and result in large anisotropies. However, these anisotropies are

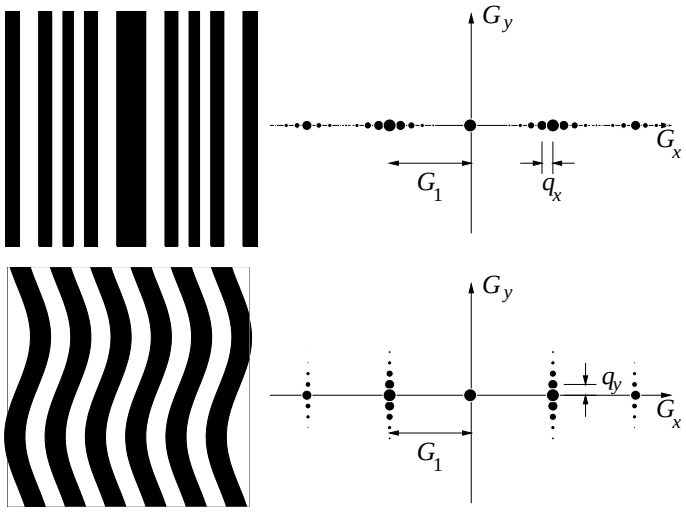

Fig. 4. Low energy perturbations of the UCDW. Top: The longitudinal modulation. Bottom: The transverse modulation. On each panel, the right-hand side shows the Bragg peaks of $\Delta(\mathbf{G})$ in reciprocal space. G_1 is the wavevector of the UCDW, and q_x, q_y are the wavevectors of the modulation. See Eqs. (6)–(9).

not seen until the temperature is an order of magnitude smaller than the energy gained in the stripe formation. We are thus compelled to investigate the properties of such stripes at low temperatures, in the hope that it is not their *formation*, but rather the thermodynamics of the different configuration of *pre-existent* stripes which is responsible for the observed anisotropic-isotropic transition.

To study this behavior, we consider the low energy states which correspond to long wavelength fluctuations of the UCDW (care must be taken that the modulations of the stripes do not accumulate charge over large distances, which would greatly increase the Coulomb energy of the system). Such modulations can be, in general, described by a distortion of the UCDW stripe edges of the form[47]

$$u(x, y) = \alpha \cos(q_x x) \cos(q_y y) \,, \tag{5}$$

where α, $\mathbf{q}$ are the amplitude and wavevector of the modulation. Figure 4 illustrates longitudinal ($q_y = 0$) and transverse ($q_x = 0$) modulations. These modulations increase the energy of the system by adding "Bragg peaks" to $\Delta(\mathbf{G})$ in regions other than the minimum of the Coulomb interaction $U(\mathbf{G})$ [See Eq. (4)].

For a perturbation of the form above [Eq. (5)], the energy gain per unit area can be readily calculated to $\mathcal{O}[\alpha^2]$. In the long-wavelength limit, keeping the lowest order (in q) non-trivial terms we find

$$\Delta\mathcal{E} = \frac{\alpha^2}{8}[Bq_x^2 + Kq_y^4] \,, \tag{6}$$

with the elastic coefficients given by

$$B = \frac{\nu^*}{2\pi l_b^2} \frac{G_1^2 \partial^2 E^{\mathrm{ucdw}}}{\partial G_1^2}\,, \tag{7}$$

and

$$K = \frac{1}{16\pi^3 l_b^2} \sum_{j=-\infty}^{\infty} \frac{\sin^2(\pi\nu^* j)}{j^2} \left[U''(G_1 j) - \frac{U'(G_1 j)}{G_1 j}\right]. \tag{8}$$

It is easy to see from energetics above [Eq. (6)] that the low-energy perturbations of a UCDW correspond one-to-one to those of a smectic liquid crystal:[49]

$$E_{\mathrm{sm}} = \frac{1}{2}\int d^2r [B(\partial_x u)^2 + K(\partial_y^2 u)^2]\,. \tag{9}$$

Results for the elastic moduli B and K are presented in Table 1 for parameters relevant to the sample used in Refs. 32–35. [Possible higher order elastic terms in Eq. (9) are not expected to be relevant since they only become large for momenta near the edge of the Brillouin zone, where the validity of the elastic theory is doubtful.[47]]

The energy functional for a smectic [Eq. (9)] has been extensively studied. We follow closely the formulation of Toner and Nelson.[49] Since the dimensionality of the system ($d = 2$) is one below the lower critical dimension for layered materials, phonon fluctuations readily destroy positional order for $T > 0$ (the Landau–Peierls argument), while preserving order in the layer orientation. However, this argument omits dislocations, which have finite energy; their energy can be estimated as[47]

$$E_D = \frac{Ba^2}{4\pi}[\sqrt{2q_c\lambda + 1} - 1]\,, \tag{10}$$

where $\lambda^2 = K/B$ and $q_c \sim \pi/a$ is a large momentum cut-off. Therefore, for $T > 0$ we expect a density of dislocations given by $n_D \approx a^{-2} e^{-E_D/k_B T}$. At distances larger than $\xi_D = n_D^{-1/2}$, and as long as $E_D \not\gg k_B T$, dislocations can be treated in a Debye–Hückel approximation. Then, to lowest order in q_x^2 and q_y^2, the correlation function for the layer normal angle $\theta = -\partial_y u$ can be written as[49]

$$\langle\langle \tilde{\theta}(\mathbf{q})\tilde{\theta}(-\mathbf{q})\rangle\rangle = \frac{k_B T}{2E_D q_x^2 + K q_y^2}\,, \tag{11}$$

which is the correlation function of a two-dimensional nematic, with a free energy

$$F_{\mathrm{nm}} = \frac{1}{2}\int d^2r [K_1(\nabla\cdot\mathbf{n})^2 + K_3[\mathbf{n}\times(\nabla\times\mathbf{n})]^2]\,, \tag{12}$$

where $\mathbf{n} = (\cos\theta, \sin\theta)$ is the director field, and the Frank constants are given by $K_1 = K$ and $K_3 = 2E_D$. Orientational correlations in the director $\mathbf{n}(\mathbf{r})$ should decay algebraically at distances much larger than ξ_D. Table 2 summarizes the values of K_1 and K_3. The values of these elastic constants are determined at distances comparable to ξ_D ($\sim$10 a at $T \sim 100$ mK).

At sufficiently long wavelengths, Nelson and Pelcovits,[59] using a momentum-shell renormalization approach, have shown that deviations from the one-Frank

Table 2. Frank elastic constants K_1 and K_3, renormalized elastic constant K and KT disclination unbinding temperature calculated for the experimental realization of Refs. 32–35. Note the characteristic oscillations with the spin index.

ν	σ	K_1 (mK)	K_3 (mK)	K (mK)	T_{KT}(mK)
9/2	↑	189	1030	610	206
11/2	↓	144	783	463	156
13/2	↑	192	1041	616	208
15/2	↓	158	848	503	170
17/2	↑	196	1034	615	208
19/2	↓	167	875	521	176

constant approximations $K_1 = K_3$ are irrelevant, and the system is equivalent to a two-dimensional XY model:

$$F_{\rm xy} = \frac{1}{2} K(T) \int d^2 r (\nabla\theta)^2 \,, \tag{13}$$

with $K \to [K_1(\xi_D) + K_3(\xi_D)]/2$ at very large distances. For our values of K_1 and K_3, at the characteristic temperatures of the experiments, convergence is achieved at distances around 20–100 ξ_D. We then expect unbinding of disclination pairs at the KT temperature:[50–53]

$$k_B T_{KT} = \frac{\pi}{8} K(T_{KT}) \,, \tag{14}$$

where the $\pi/8$ comes instead of the more common $\pi/2$ for vortices since each disclination winds up the angle by π rather than 2π. In general, $K(T_{KT})$ corresponds to the large-distance elastic constant (reduced by disclination pairs) to the bare elastic constant at small distances $K(0)$ by means of the KT RG formulas.[50–53] In practice, the polarization of the "elastic medium" reduces the magnitude of the elastic constant so that $k_B T_{KT} \simeq 0.86(\pi/8)K(T=0)$.[47]

Table 2 presents the resulting estimates for the disclination unbinding transition temperatures for half-filled LL-s. Although these can only be considered estimates due to the approximations used, they are in qualitative agreement with the temperatures at which the anisotropies are seen to vanish.[32–35] For comparison, Fradkin *et al.*[48] find $T_{KT} \simeq 65$ mK with significant rounding by 5% intrinsic anisotropy for $\nu = 9/2$ by fitting the results of a Monte-Carlo simulation of an XY model to the resistivity data of Ref. 32–35. We also see the characteristic spin oscillation of the transition parameters.[32–35]

5. Broken Rotational Symmetry States at the Quantum Level

Although the quantum Hall smectic/nematic theory based on CDW-s and the Hartree–Fock approximation presented earlier is very appealing, an orientationally ordered QHN liquid state is *sufficient* in order to account for the observed transport anisotropies, since a nematic state would break rotational symmetry while

preserving translational symmetry. There are different ways to build nematic liquid crystalline states. One may consider first a smectic liquid state where both the rotational and translational symmetries are spontaneously broken and then assume that through the Landau–Peierls mechanism (or even through dislocation unbinding) the smectic state melts into a nematic liquid crystalline state with broken rotational symmetry, but otherwise with restored translational invariance. In this approach the QHN state can be visualized as a melted smectic, namely a smectic with dislocations. This is, in essence, the path presented in Sec. 4.

An alternative route to build a QHN state from the isotropic and weakly correlated side is to consider the zero-temperature isotropic to nematic transition as a Fermi surface instability[60] where the Fermi surface changes from circular (isotropic) to elliptical (anisotropic). Experiments studying the longitudinal propagation of sound would be an accurate probe of this scenario, since the behavior of the sound waves in the nematic ordered state would be dramatically different from that in the isotropic Fermi liquid state.[61] So far the answer is not conclusive.

Another approach is to start from a nematic liquid state, assuming that the rotational symmetry is already broken by some, yet unknown, symmetry-breaking field. A theory of such QHN phase was recently introduced by Radzihovsky and Dorsey[62–64] and is guided by the chiral edge dynamics of the local smectic layers and describes the local orientational order of the QHN by a unit director field which is also coupled to a symmetry-breaking field. The result is the prediction of the existence of a novel director-density mode, with highly anisotropic dispersion, which remains gapless even in the presence of an ordering field.

The experimental discovery of magnetotransport anisotropy in higher Landau levels around filling factors $\nu = 2L + 1/2$ poses challenging questions on the true microscopic nature of such states and their relationship to the parent CF states originating from $\nu = 2L + 1/3$. Clearly the specific value of L plays a major role and even determines the onset of anisotropy. The importance of L to anisotropy is evident if one considers states with filling factor $\nu = 1/2$, $5/2$ and $9/2$. In such a case we know that the $\nu = 1/2$ ($L = 0$) state is an isotropic compressible Fermi liquid; the $\nu = 5/2$ ($L = 1$) state is an isotropic incompressible FQHE-like liquid; and the $\nu = 9/2$ ($L = 2$) state is an anisotropic compressible liquid state. The same does not apply to states with filling factors $\nu = 1/3$, $2 + 1/3$ and $4 + 1/3$, even though the $4 + 1/3$ state is close (within the $\Delta\nu = 0.2$ range) to filling factors around $\nu = 9/2 = 4 + 1/2$ where signs of anisotropy can still be observed.

A fundamental question that arises concerns the microscopic nature and how to construct an anisotropic state that describes arbitrary states at any given filling factor including the LLL Laughlin filling factors at $\nu = 1/3$ and $\nu = 1/5$. Such an anisotropic state may be translationally invariant, but should have *broken rotational symmetry (BRS)* in order to have anisotropic properties. The interest of building a microscopic anisotropic wave function for liquid crystalline electronic phases in the LLL is not purely academic, but is inspired from the classical 2D melting theory

of the classical two-dimensional one-component-plasma (2DOCP). The Kosterlitz, Thouless, Halperin, Nelson and Young (KTHNY) theory[50–53,65,66] of the classical 2D melting problem predicts that an intermediate *third phase* called *hexatic*, will exist between the hexagonal solid and the liquid phases in a certain portion of the phase diagram as temperature decreases. Similarly, an intermediate *nematic* could exist between some kind of anisotropic crystal and an isotropic liquid. There is no long-range translational or rotational order (the system is both translationally and rotationally invariant) in the liquid phase, while the system has quasi-long-range translational and true long-range rotational order in the solid phase. The hexatic phase in the KTHNY theory is thought to have no true long-range translational order, but does retain quasi-long-range orientational order (the system is translationally invariant, but not rotationally invariant at least for short distances). The quantum Hall regime counterpart of the temperature in the classical 2D melting problem is the electronic filling factor. A transition to a quantum Wigner crystal (WC) state in the LLL is achieved by reducing the filling factor and we know that the WC states stabilize for $\nu_c \leq 1/6.5$. Inspired by the KTHNY theory, it makes perfectly sense to investigate the possibility of intermediate liquid crystalline mesophases in the LLL stabilizing during a liquid-to-solid phase transition before the full onset of Wigner crystallization.

Liquid crystalline phases with no translational order but with quasi-long-range orientational order may possess different forms of rotational group symmetry. For simplicity we select a small set of possible rotational symmetry groups: C_2, C_4, and C_6 which correspond to a *nematic*, *tetratic* and *hexatic* phase, respectively. If we want to describe BRS liquid crystalline states in the LLL there are some basic requirements to be followed:

(i) the states must obey Fermi statistics;
(ii) the states must be translationally invariant (at least far away from the boundaries for finite systems);
(iii) there must be a BRS belonging to the proper rotational symmetry group; and
(iv) the states must belong to the LLL Hilbert space.

If one is able to build BRS liquid crystalline states in the LLL, extension of such states at *any* higher LL with index $L \geq 1$ is straightforward and various properties at *any* LL can be readily obtained from properties calculated in the LLL.

The so-called BRS wavefunctions are a special class of liquid crystalline wave functions that satisfy all the above requirements.[67–72] They are systematically constructed by splitting the zero-s of the isotropic Laughlin liquid state according to the proper rotational symmetry group in consideration in a way that conserves the anti-symmetry (Fermi statistics) and translational invariance, but breaks the rotational invariance of the wave function (see Fig. 5). The introduction of a preferred set of directions into the wave function creates a necessary degree of anisotropy. A generalized liquid crystalline wave function for LLL filling factors $\nu = 1/m$ can be

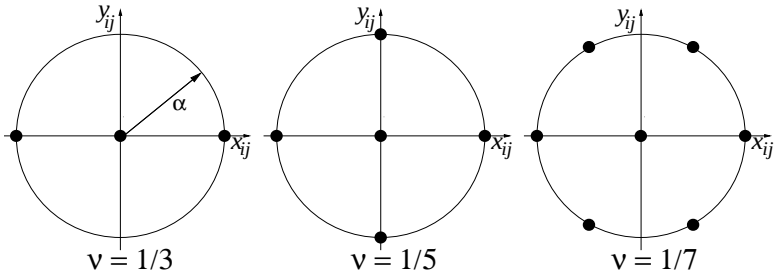

Fig. 5. Nodal distribution for $z_{ij} \equiv z_i - z_j$ for a quantum Hall *nematic* at $\nu = 1/3$, *tetratic* at $\nu = 1/5$, and *hexatic* at $\nu = 1/7$.

written as:

$$\Psi_{\alpha}^{1/m} = \left\{ \prod_{i<j}^{N} \left[\prod_{\mu=1}^{m-1} (z_i - z_j - \alpha_\mu) \right] \right\} \times \prod_{i<j}^{N} (z_i - z_j) \exp\left(-\sum_{k=1}^{N} \frac{|z_k|^2}{4l_0^2} \right), \qquad (15)$$

where $z_k = x_k + iy_k$ is electron's position in complex notation, $l_0 = \sqrt{\hbar/(eB)}$ is electron's magnetic length, $-e$ ($e > 0$) is electron's charge, B is a perpendicular magnetic field in the z direction, $\hbar$ is the reduced Planck's constant, N is the total number of electrons, $m = 3, 5, 7$ is an odd integer, and α_μ is the set complex directors distributed in pairs of opposite value to satisfy Fermi statistics. For simplicity, we focus on liquid crystalline BRS states with the highest possible level of discrete rotational symmetry for each filling factor in which the α_μ-s are symmetrically distributed in a circle around the origin (see Fig. 5):

$$\alpha_\mu = \alpha e^{i2\pi(\mu-1)/(m-1)}, \quad \mu \in \{1, 2, \ldots, (m-1)\}. \qquad (16)$$

Without loss of generality α can be taken to be real. The BRS liquid crystalline wavefunction in Eq. (15) represents a translationally, but not rotationally invariant liquid crystalline state for filling factors corresponding to $\nu = 1/m$, is antisymmetric, lies entirely in the LLL, and reduces to the isotropic Laughlin liquid state when the anisotropy parameter, α, vanishes.

5.1. *Model and investigation of BRS states*

We consider a two-dimensional (2D) model of N electrons subjected to a strong perpendicular magnetic field. The electrons are embedded in a neutralizing background of positive charge with uniform density $\rho_0 = \nu/(2\pi l_0^2)$ spread within a finite disk with radius R_N and area $\Omega_N = \pi R_N^2$. The electrons can move freely all over the 2D space and are not restricted to stay inside the disk. Since the uniform density of the neutralizing positive charge of the disk is defined as $\rho_0 = N/\Omega_N$ one can write the radius of the disk in terms of the electronic length as $R_N = l_0\sqrt{2N/\nu}$.

Since the BRS wave functions introduced in Eq. (15) describe a liquid crystalline state in the LLL, the kinetic energy per electron is a mere constant: $\langle \hat{K} \rangle / N =$

$\hbar\omega_c/2$, where ω_c is the cyclotron frequency. Thus, the properties of the system are determined by the potential energy:

$$\hat{V} = \hat{V}_{ee} + \hat{V}_{eb} + \hat{V}_{bb}\,, \tag{17}$$

where $\hat{V}_{ee}, \hat{V}_{eb}$ and $\hat{V}_{bb}$ are the electron-electron, electron-background and background-background potential energy operators, respectively.

The interaction potential between a pair of two electrons with 2D coordinates $\vec{r}_i$ and $\vec{r}_j$ takes the form:

$$v(r_{ij}) = \frac{e^2}{\epsilon}\,\frac{1}{\sqrt{r_{ij}^2 + \lambda^2}}\,, \tag{18}$$

where $r_{ij} = |\vec{r}_i - \vec{r}_j|$ is the distance between the two electrons and λ is a phenomenological length parameter. This interaction potential is more general than the bare Coulomb interaction potential and takes into consideration the finite thickness of the quasi-2D electron system[73] through the parameter λ. When $\lambda = 0$ the above phenomenological potential reduces to the bare Coulomb potential.

Since the involved potentials are one- and two-body potentials, the system is accurately solved if we can determine all one- and two-body distribution functions, i.e. the *density* $\rho(\mathbf{r}) \equiv \langle \sum_{i=1}^{N} \delta(\mathbf{r}_i - \mathbf{r})\rangle$, and the *pair correlation function* $g(\mathbf{r}_{12}) \equiv \rho_0^{-2}\langle \sum_{i\neq j}^{N} \delta(\mathbf{r}_i - \mathbf{r}_1)\delta(\mathbf{r}_j - \mathbf{r}_2)\rangle$, respectively. The determination of these distribution functions enables an accurate calculation of all potential energy terms in the thermodynamic limit. A calculation of the static structure factor,

$$S(\mathbf{q}) - 1 = \rho_0 \int d^2 r_{12} e^{-i\mathbf{q}\cdot\mathbf{r}_{12}}[g(\mathbf{r}_{12}) - 1] \tag{19}$$

is also useful. Because of the anisotropy of the BRS wave function for $\alpha \neq 0$, both the pair correlation function and the static structure factor are explicitly angle-dependent, namely: $g(\mathbf{r}_{12}) = g(r_{12}, \theta)$ and $S(\mathbf{q}) = S(q, \theta_q)$ for $\alpha \neq 0$.

An accurate calculation of BRS liquid crystalline state energies in the thermodynamic limit is necessary to judge the zero-temperature stability of the BRS liquid crystalline states with respect to the isotropic liquid states. In the thermodynamic limit, the ground state correlation energy per particle can be easily computed from

$$E_\alpha = \frac{\langle \hat{V}\rangle}{N} = \frac{\rho_0}{2}\int d^2 r_{12} v(r_{12})[g(\mathbf{r}_{12}) - 1]\,. \tag{20}$$

Therefore, a good estimate of the correlation energy in the thermodynamic limit requires an accurate computation of $g(\mathbf{r}_{12})$, for example, by means of Monte-Carlo (MC) simulations methods[74,75] or other techniques.

The correlation energy may also be computed from the static structure factor:

$$E_\alpha^{(L)} = \frac{1}{2}\int \frac{d^2 q}{(2\pi)^2}\,\tilde{v}(\mathbf{q})[S(\mathbf{q}) - 1] \times [L_L(q^2/2)]^2\,, \tag{21}$$

where the multiplication by the Laguerre polynomial allows for the calculation of the correlation energy in the Lth LL.[69–72,75]

5.2. *BRS Laughlin states*

Monte-Carlo (MC) simulation methods were used to study the possibility of a BRS liquid crystalline state for the leading Laughlin states at filling factors, $\nu = 1/3$, $1/5$ and $1/7$. A BRS trial wave function as in Eq. (15) was considered and various properties were analyzed as function of the anisotropic parameter α.

In order to determine the pair distribution function $g(\mathbf{r})$, we perform standard MC simulations in disk geometry using the Metropolis algorithm.[76] The electronic configurations are sampled from the probability distribution given by:

$$P(\mathbf{r}_1, \ldots, \mathbf{r}_N) \equiv |\Psi_\alpha^{1/m}(\mathbf{r}_1, \ldots, \mathbf{r}_N)|^2 \,, \tag{22}$$

where we omitted irrelevant normalization constants.

For each α under consideration, we start by uniformly distributing N electrons inside of a disk of radius R_N. In each MC step, electrons are randomly moved by a given amount (chosen in the beginning of the run so that approximately 50% of the MC attempts are successful). The move is accepted if $P^{\rm new}/P^{\rm old}$ is larger than a random number between 0 and 1, and otherwise rejected. After an initial "thermalization" process, the $g(\mathbf{r})$ was computed for up to $N = 400$ electrons and the results were extrapolated to the thermodynamic limit. Care is taken so that only electrons in the "bulk" of this system are counted (by excluding a ring near the periphery of the disk).[75] Direct calculations of the correlation energy in the LLL for various potentials were also performed to further verify our results.

Extensive MC simulations in disk geometry have allowed us to determine very accurately the pair distribution function and the static structure factor. In order to compare the isotropic Laughlin's liquid state ($\alpha = 0$) with the BRS liquid crystalline states ($\alpha \neq 0$) we studied the properties of the BRS wave functions while varying the anisotropy parameter, α.

The interaction potential of Eq. (18) was considered. This choice is motivated by the well-known fact that the finite layer thickness of a real 2D system leads to a weakening and eventual collapse of the FQHE.[77] When λ increases as to become larger than the magnetic length, the short-range part of the modified Coulomb interaction softens and as a result there is a possibility that the isotropic FQHE liquid state may become unstable with respect to another state of different nature (a Wigner crystal can be an obvious choice, but a possible new candidate can be the BRS liquid crystalline state considered here).

In order to compare the energy of the isotropic Laughlin liquid state with that of an anisotropic BRS liquid crystalline state, an accurate computation of the pair correlation function for different α-s is performed. For small α's, MC simulations with $N = 196$ electrons were sufficient to give a very accurate pair distribution function. For larger α-s (that induce sizable oscillations in the density), MC simulations with as many as $N = 400$ electrons were needed.

Figure 6 shows a typical snapshot of an electronic configuration sampled during our MC simulations with large α-s. The apparent charge density wave (CDW)-like

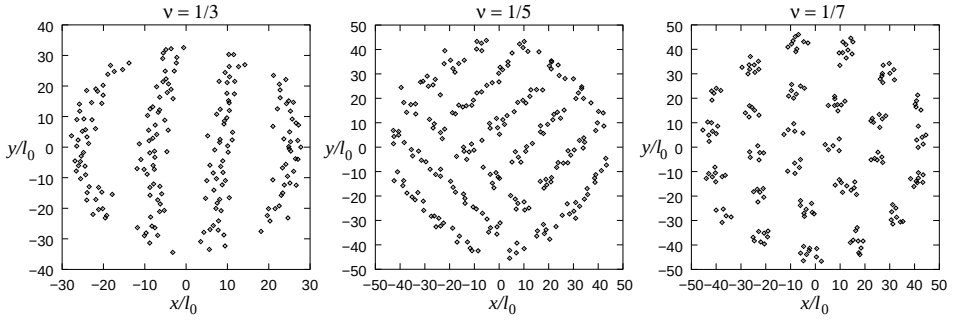

Fig. 6. Typical electron configurations for a nematic ($\nu = 1/3$, $\alpha = 7$, left panel), tetratic ($\nu = 1/5$, $\alpha = 8$, center panel), and hexatic ($\nu = 1/7$, $\alpha = 10$, right panel).

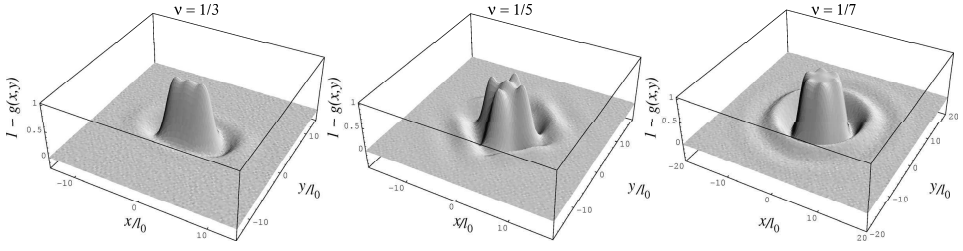

Fig. 7. Pair correlation function $g(\mathbf{r})$ for $\nu = 1/3, \alpha = 2$ (left panel), $\nu = 1/5, \alpha = 3$ (center panel), $\nu = 1/7, \alpha = 3$ (right panel). Note the discrete rotational symmetry of each state. Results are from MC simulations in a disk geometry.

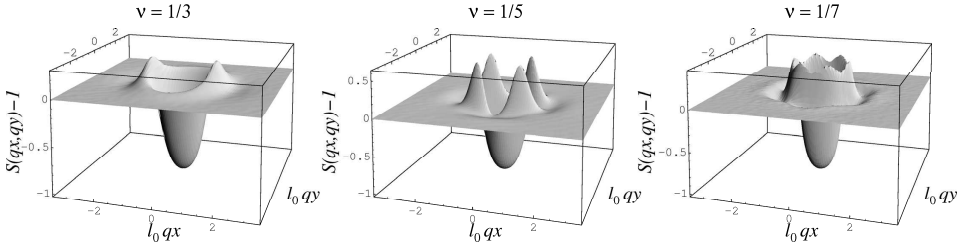

Fig. 8. Static structure factor $S(\mathbf{q})$ for $\nu = 1/3, \alpha = 2$ (left panel), $\nu = 1/5, \alpha = 3$ (center panel), $\nu = 1/7, \alpha = 3$ (right panel). Note the discrete rotational symmetry of each state.

structures on the BRS liquid crystalline phase are visible only due to the extremely large α-s used to permit visualization of the anisotropy (see Ref. 72 for more details).

Figure 7 displays the calculated the pair distribution function, $g(\mathbf{r})$, for the BRS Laughlin states at filling factors: $\nu = 1/3$, $\alpha = 2$ "*nematic*", $\nu = 1/5$, $\alpha = 3$ "*tetratic*", and $\nu = 1/7$, $\alpha = 3$ "*hexatic*". Each MC simulation involves systems with $N = 400$ electrons.[72]

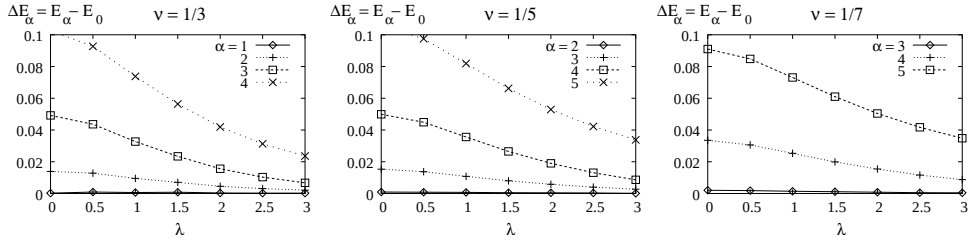

Fig. 9. Energy difference between anisotropic states and the isotropic state ($\alpha = 0$) $\Delta E_\alpha \equiv E_\alpha - E_0$ for filling factors $\nu = 1/3$, $1/5$ and $1/7$ in the LLL. These results are plotted as function of the quasi-2D layer thickness λ. Energies are in units of $e^2/(\epsilon l_0)$.

Figure 8 shows the corresponding static structure factors $S(\mathbf{q})$ for the BRS liquid crystalline states at filling factors $\nu = 1/3$, $1/5$ and $1/7$ for selected values of α.[72]

The energy differences, $\Delta E_\alpha = E_\alpha - E_0$ between the anisotropic BRS liquid crystalline states ($\alpha \neq 0$) and the isotropic liquid state ($\alpha = 0$) for states with LLL filling factors $\nu = 1/3$, $1/5$ and $1/7$ are presented in Fig. 9. For small values of $\alpha \in (0, \approx 2]$, the BRS liquid crystalline states have an energy only slightly above the Laughlin liquid states ($\alpha = 0$), however for larger α-s this difference increases.

Based on the calculated energies, we conclude that, for the case of the bare Coulomb interaction potential ($\lambda = 0$) and for the case of finite thickness modified Coulomb potential ($\lambda \neq 0$), the uniform isotropic liquid state is energetically more favorable than the BRS anisotropic liquid crystalline state at all LLL Laughlin filling factors of the form: $\nu = 1/3, 1/5$ and $1/7$. Since it is known that the onset of Wigner crystallization occurs at filling factors $\nu_c \leq 1/6.5$ these results strongly suggest that a BRS liquid crystalline phase (at least of the form considered in this work) is not stable as the ground state in the LLL for filling factors $0 < \nu \leq 1$.

The situation changes dramatically in higher LL-s. The properties of BRS Laughlin states in higher Landau levels with filling factor, $\nu = 2L + 1/m$ where $L = 0, 1, \ldots$ and $m = 3, 5, 7$ can be immediately derived from the properties of BRS Laughlin states in the LLL ($L = 0$). If transitions to other LL-s are neglected (i.e. a *single-LL approximation*), the pair distribution function, $g(\mathbf{r})$ and the static structure factor, $S(\mathbf{q})$ in higher LL-s ($L \neq 0$) are related to those at the LLL ($L = 0$) by means of a convolution or product respectively. We use this approximation (which, moreover, quenches the kinetic energy in higher LL-s as well). It is then sufficient to use distribution functions calculated in the LLL to obtain the correlation energy per electron in an arbitrary LL with index $L \neq 0$ [see Eq. (21)].

In particular, we focus our attention on the Laughlin state $\nu = 2L + 1/3$ which is the closest Laughlin state to the half filled state $\nu = 2L + 1/2$. Such state also happens to be in border of the range of filling factors, $\Delta\nu = 0.2$ around 1/2-filled upper Landau levels where signatures of anisotropy (although very weakened) still persist. In what follows we use the static structure factor, $S(\mathbf{q})$ previously computed

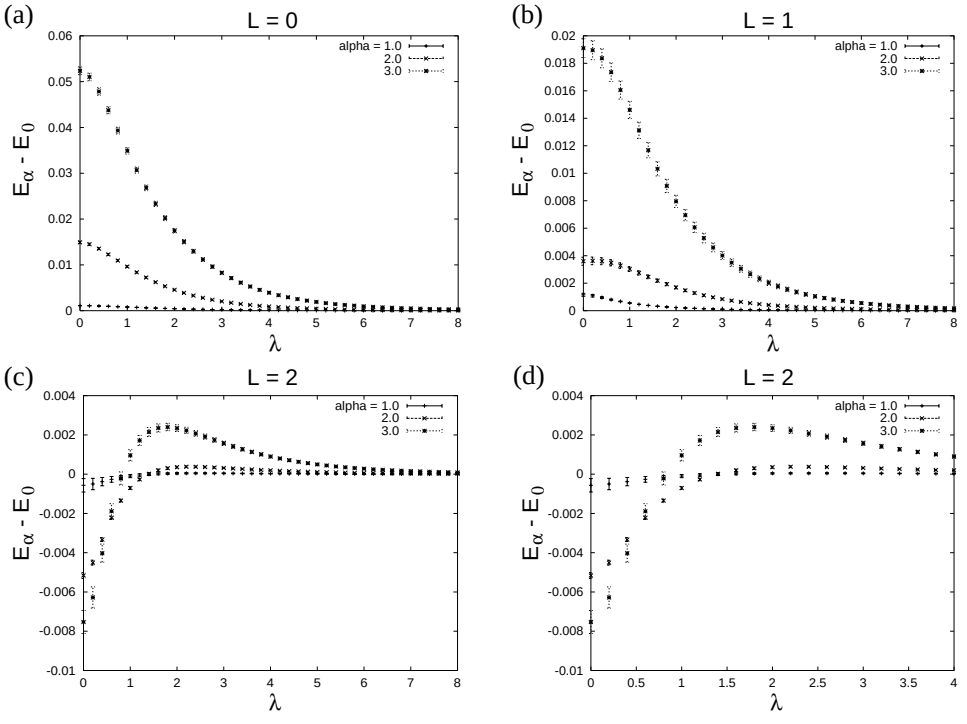

Fig. 10. Correlation energy per particle in BRS states with $\alpha = 1, 2$ and 3 relative to the isotropic ($\alpha = 0$) state for t indices of Landau levels L as function of the short-distance cut-off parameter λ. All energies are in units of $e^2/(\epsilon l_0)$. (a) Lowest LL ($L = 0$); (b) First excited LL ($L = 1$); (c) Second excited LL ($L = 2$) (d) Detail of (c). Note that there are ranges of λ for which BRS liquid crystalline states are favorable in the last case ($L = 2$).

through MC simulations for LLL BRS liquid crystalline wave functions in order to obtain the correlation energies, $E_\alpha^{(L)}$ for various high LL-s.

Figure 10 shows the energy difference between BRS states with $\alpha = 1$, 2 and 3, and the isotropic state with $\alpha = 0$. Our findings indicate that in the LLL ($L = 0$) the isotropic Laughlin state is stable for all λ we considered, since all $\alpha \neq 0$ states have higher energies (top panel). This results are in disagreement to those of Ref. 68 and 69 and coincide *quantitatively* with our previous hypernetted-chain (HNC) calculations.[69] We also observe stability of the isotropic state in the first excited LL ($L = 1$, $\nu = 2 + \frac{1}{3}$). The situation changes considerably in the second excited LL-s ($L = 2$, $\nu = 4 + \frac{1}{3}$) where, for a considerable range of the short-distance cut-off parameter, λ, BRS states are found to have *lower* energies and the incompressible Laughlin-like state is unstable toward a nematic state (see lower panels of Fig. 10).

The only significant sources of error in the MC calculations arise from the statistical errors due to finite sampling and the discrete nature of the grid used in the determination of the pair distribution function $g(\mathbf{r})$ (these errors are inherent

to all MC methods). The errors propagate to the static structure factor $S(\mathbf{q})$, and are amplified at large-q by the Laguerre polynomials in Eq. (21). The error bars in Fig. 10 are estimated by comparing our $S(\mathbf{q})$ to analytical approximations calculated (for the isotropic state) by Girvin MacDonald and Platzman[78,79] (for the isotropic case, $\alpha = 0$).

The above results suggest that an isotropic liquid state is energetically favorable in the LLL ($L = 0$) and the first excited LL ($L = 1$), but an anisotropic BRS liquid crystalline state is more stable in the second excited LL ($L = 2$). This fact is also in agreement with experimental findings of strong magnetotransport anisotropy only at Landau levels with index $L \geq 2$. A qualitative explanation for this is simple: In the LLL the electron packets are simple gaussians, and it is clear that the best way to minimize their Coulomb repulsion is by placing the vortices responsible for the CF transformation[4,5,9] (see also footnote a) precisely at the location of the electron themselves ($\alpha = 0$). However, in higher LL-s, the wavepackets take a more "ring-like" shape, and a finite α permits a more optimal distribution of charge resulting in a lower energy of the anisotropic $\nu = 4 + 1/3$ state relative to the isotropic $\nu = 4 + 1/3$ counterpart.

5.3. *BRS half-filled state*

The HLR theory argues that a 2D strongly correlated electronic system subjected to a perpendicular magnetic field at which the LLL is half-filled is mathematically equivalent with system of fermions interacting with a Chern–Simons gauge field such that the average effective magnetic field acting on the fermions is zero.[19] At precisely $\nu = 1/2$ the fermions do not see a net magnetic field therefore they form a 2D Fermi sea of uniform density much like the ideal 2D Fermi gas. Therefore the quantum state at $\nu = 1/2$ should have a nature that resembles a compressible isotropic Fermi-liquid-like phase.

A microscopic description of the LLL half-filled state has been provided by Rezayi and Read[80] (RR) in terms of a correlated Fermi liquid wave function that is a product of a Slater determinant of 2D plane waves with a Bose–Laughlin half-filled wave function:

$$\Psi(\mathbf{r}_1, \ldots, \mathbf{r}_N) = \hat{P}_0 \prod_{j<k}^{N} (z_j - z_k)^2 \exp\left(-\sum_{k=1}^{N} \frac{|z_k|^2}{4l_0^2} \right) \det[\varphi_{\mathbf{k}}(\mathbf{r}_i)]\,, \qquad (23)$$

where the Slater determinant, $\det[\varphi_{\mathbf{k}}(\mathbf{r}_i)]$ consists of 2D plane waves for spin polarized electrons, $\varphi_{\mathbf{k}}(\mathbf{r}_i)$ that fill a 2D Fermi disk with Fermi momentum up to k_F and $\hat{P}_0$ is a projection operator onto the LLL ($L = 0$) that acts upon the whole wave function.

To obtain a BRS liquid crystalline wave function at filling $\nu = 1/2$ of the LLL[81] we add an anisotropic symmetry breaking parameter α to the RR

wave function:

$$\Psi_\alpha(\mathbf{r}_1,\ldots,\mathbf{r}_N) = \hat{P}_0 \prod_{j<k}^{N} (z_j - z_k + \alpha)(z_j - z_k - \alpha) \exp\left(-\sum_{k=1}^{N} \frac{|z_k|^2}{4l_0^2}\right) \det[\varphi_{\mathbf{k}}(\mathbf{r}_i)]\,. \tag{24}$$

The half-filled BRS liquid crystalline wavefunction describes a translationally invariant Fermi liquid-like state. For $\alpha \neq 0$ the rotational symmetry is broken and the state has nematic order with α interpreted as the nematic director. For $\alpha = 0$ we recover the isotropic RR Fermi liquid wavefunction where the rotational symmetry is restored. If we consider α to be real the system will have a stronger modulation in the x-direction, and therefore likely have larger conductance in the perpendicular direction: $\sigma_{yy} > \sigma_{xx}$. This wavefunction is an obvious starting point to study the *nematic* BRS quantum Hall liquid crystalline states at half filling since it can be further generalized to half filled states in higher Landau levels with filling factors, $\nu = 2L + 1/2$, where $L = 0, 1, 2, \ldots$ is the Landau level index. In the $L \neq 0$ case the projector operator $\hat{P}_L$ should be used instead of $\hat{P}_0$.

The general BRS half-filled wave function of Eq. (24) is rather complex, nevertheless one notes that if the projection operator, $\hat{P}_0$ is disregarded then its form becomes a standard Jastrow–Slater form. A method suitable to carry out calculations for Jastrow–Slater wave functions which gives physical quantities, such as energy, pair distribution function, static structure factor, etc. exactly in the thermodynamic limit is the so-called Fermi hypernetted-chain (FHNC) method.[82–90]

This method allows us to compute physical quantities in the thermodynamic limit, without the limitations of using a finite number of particles that hinder other techniques, where the extrapolation of the results to the thermodynamic limit is not totally unambiguous. The neglect of certain type of terms, called elementary diagrams is a necessary approximation generally incorporated in the otherwise FHNC method (FHNC/0).[81] In our study of the BRS half-filled liquid crystalline wave function [Eq. (24)] we resort to the approximation of neglecting the LLL projection operator, $\hat{P}_0$, therefore we use the "unprojected" version of the wave function. Under these conditions we applied the FHNC/0 method and studied the stability of the BRS liquid crystalline state at $\nu = 1/2$ with respect to its isotropic liquid counterpart. The FHNC/0 allowed us to determine quickly and with reasonable accuracy the pair distribution function and the static structure factor.

In Fig. 11 we plot the pair distribution function $g(\mathbf{r})$ for $\alpha = 2$ [panels (a) and (b)], and the angle-averaged pair distribution function $g_{av}(r)$ corresponding to $\alpha = 0$, 1, 2, 2.5 and 3 [panels (c) and (d)]. It is interesting to note, for $\alpha \neq 0$, the noticeable angle-dependence of $g(\mathbf{r})$, and the splitting of the triple node at the origin to a simple node at the origin and additional simple nodes at $r = \alpha$ and angle $\theta = \theta_\alpha$, $\theta_\alpha + \pi$ ($\theta_\alpha = 0$ in this case).

In Fig. 12 we plot the static structure factor $S(\mathbf{q})$ for $\alpha = 2$ (top panel), where the most important feature is the emergence of peaks in $S(\mathbf{q})$ characteristic of a

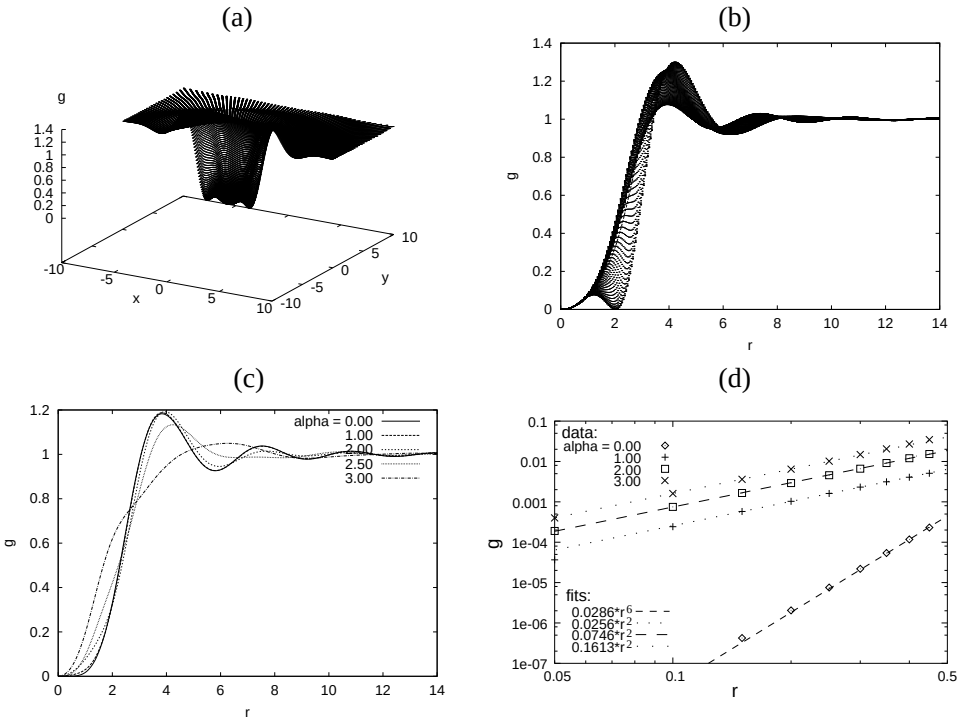

Fig. 11. Pair distribution function for the BRS state at $\nu = 1/2$. (a) $\alpha = 2$, surface plot of $g(\mathbf{r})$ (the surface for $y < 0$ was removed for clarity); (b) $\alpha = 2$, dotted lines: $g(r, \theta)$ for various $\theta \in [0, 2\pi]$, full line: angle averaged $g_{av}(r)$; (c) Angle averaged $g_{av}(r)$ for $\alpha = 0$, 1, 2, 2.5 and 3; (d) Small-r behavior of $g_{av}(r)$, lines are fitting curves. Note the discrete nodes of $g(r, \theta)$ at $r = \alpha$, $\theta = \theta_\alpha$, $\theta_\alpha + \pi$ ($\theta_\alpha = 0$ in this case). Calculations were performed in the FHNC/0 approximation.

nematic structure; and the angle-averaged static structure factor $S_{av}(q)$ corresponding to $\alpha = 0$, 1, 2, 2.5 and 3 (bottom panel). Note the considerable dependence of $S_{av}(q)$ on α: as it increases the peak is broadened and flattened, with no significant change in the small-q behavior.

In order to compare the $\alpha = 0$ isotropic Fermi liquid RR state, with the $\alpha \neq 0$ BRS liquid crystalline (nematic) state we studied the properties of the BRS wave function for several α-s with magnitudes between 0 and 3. Like before, we studied the stability of the anisotropic BRS liquid crystalline state versus the isotropic RR Fermi liquid state by comparing the energy in each of these states and find the optimum value for the anisotropy-generating parameter α. As before, the energy in any LL can be calculated using the static structure factor [Eq. (21)].

Figure 13 shows the energy difference between BRS liquid crystalline states with $\alpha = 1$, 2, 2.5 and 3, and the isotropic RR state with $\alpha = 0$ at various LL-s. Our findings indicate that in the LLL ($L = 0$) the RR isotropic Fermi liquid state is stable for any λ, given that all $\alpha \neq 0$ anisotropic states resulted with higher energies. The situation changes again in higher LL-s. For $L \geq 2$ the BRS Fermi liquid states

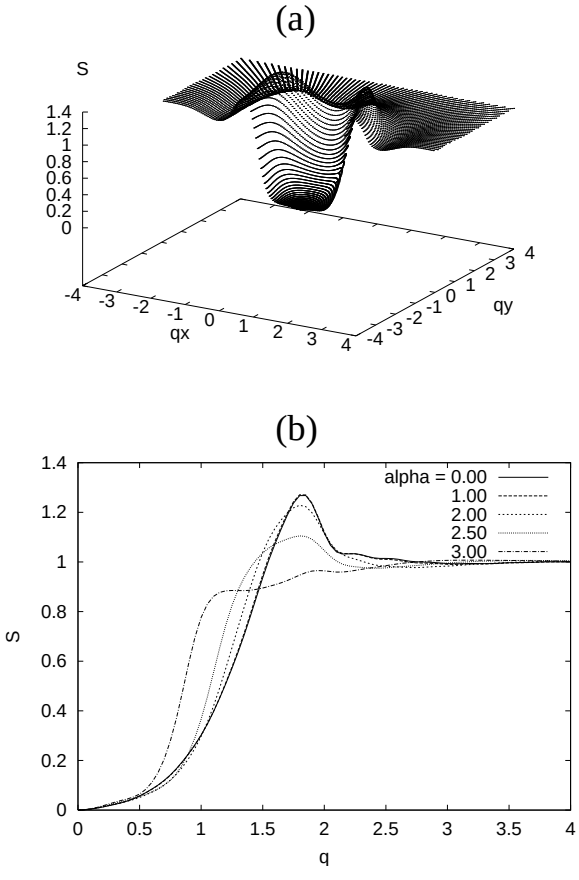

Fig. 12. Static structure factor for the BRS liquid crystalline state at $\nu = 1/2$. (a) $\alpha = 2$, surface plot of $S(\mathbf{q})$ (the surface for $q_y < 0$ was removed for clarity); (b) Angle averaged $S_{av}(q)$ for α = 0, 1, 2, 2.5 and 3. Note the presence of peaks in $S(\mathbf{q})$ consistent with a nematic structure. Calculations were performed in the FHNC/0 approximation.

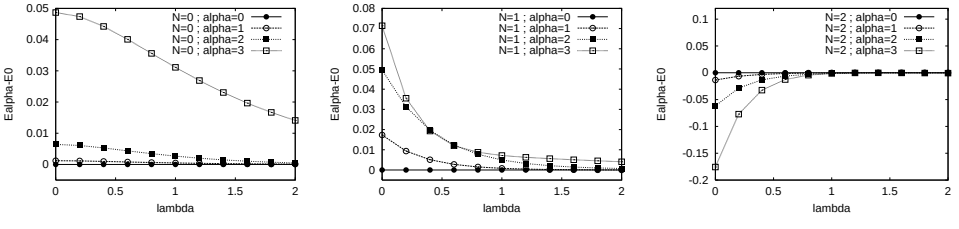

Fig. 13. Energy per particle of the Fermi BRS states with $\alpha = 1, 2$ and 3 relative to the isotropic ($\alpha = 0$) state: $E_\alpha(\lambda) - E_0(\lambda)$ for the LLL ($L = 0$) and higher LL-s as function of the short distance cut-off parameter λ. Energies are in units of $e^2/(\epsilon l_0)$. Note that for $L = 0$ and 1, the Fermi BRS states always have an energy higher than the isotropic state, whereas in higher LL-s ($L = 2$) there are ranges of λ for which Fermi BRS states are favorable.

are found to have *lower* energies and the compressible RR state is unstable towards a nematic state. The Landau index, $L = 2$, corresponds to the experimental value where anisotropy has been observed, therefore, it is likely that the BRS states proposed here are related to the low-temperature anisotropic conductance found experimentally.[32–35]

Even though we used the *unprojected* version of the BRS Fermi liquid wave function in place of its *projected* counterpart, we believe that the main conclusions that we derived will not change qualitatively when proper projection is performed, basically, for the following reasons:

(i) the presence of the Jastrow factors, already provides a considerable projection into the LLL;[91] and
(ii) energy differences will likely be accurate because the separate energies are calculated within the same approximation, therefore errors which are *systematic* will be of the same magnitude order.

6. Collective Excitations

In this section we consider the spectrum of collective excitations for the family of liquid crystalline states [Eq. (15)] proposed in Sec. 5. To calculate this excitation spectrum we use the single mode approximation (SMA),[78,79,92–95] which reliably provides the mean of the energy of the excitations that are coupled to the ground state by the density operator.[78,79,92–96] The SMA was first used in 1953 by Feynman to obtain a qualitatively correct spectrum of phonons in ^{4}He.[92,93] In the SMA, the variational wavefunction for an excitation corresponding to a density-wave is

$$\phi_{\mathbf{k}}(\mathbf{r}_1, \ldots, \mathbf{r}_N) = N^{-1/2} \rho_{\mathbf{k}} \psi_0(\mathbf{r}_1, \ldots, \mathbf{r}_N)\,, \tag{25}$$

where $\rho_{\mathbf{k}} = \sum_{j=1}^{N} e^{-i\mathbf{k}\cdot\mathbf{r}_j}$ is the density operator, and ψ_0 is the many-body ground state. The energy of this excited state can be simply evaluated:

$$\Delta(\mathbf{k}) \equiv \frac{\langle \phi_{\mathbf{k}} | H - E_0 | \phi_{\mathbf{k}} \rangle}{\langle \phi_{\mathbf{k}} | \phi_{\mathbf{k}} \rangle} = \frac{N^{-1} \langle \psi_0 | \rho_{\mathbf{k}}^{\dagger} [H, \rho_{\mathbf{k}}] | \psi_0 \rangle}{N^{-1} \langle \psi_0 | \rho_{\mathbf{k}}^{\dagger} \rho_{\mathbf{k}} | \psi_0 \rangle} \equiv \frac{f(\mathbf{k})}{S(\mathbf{k})}\,, \tag{26}$$

where $f(\mathbf{k}) = \hbar^2 k^2 / 2m$ is the "oscillator strength" and $S(\mathbf{k})$ is the static structure factor, which is directly measurable by means of neutron scattering. Using the experimental results for $S(\mathbf{k})$ and nothing else, Feynman found remarkable results, showing the phonon-like spectrum at small wavevectors, and a roton minimum at wave-vectors comparable to the inverse interatomic distance.[92,93]

In the case of fermionic systems, the SMA is also reasonably well established both for two- and three-dimensional systems in the absence of magnetic fields, yielding a decent approximation for the plasmon frequency as $k \to 0$. The application of the SMA in 2DES with a magnetic field also gives reasonable results: the magnetoplasmon at $\omega_c = eB/m_e$, result guaranteed to be exact by Kohn's theorem.[97]

In the QHE, we are mostly interested in *intra-LL* excitations, and the *inter-LL* cyclotron mode is not of interest. In 1985 Girvin, MacDonald and Platzman (GMP)

proposed an ingenious ansatz for *projected* excited states:[78,79]

$$|\psi_{\mathbf{q}}\rangle = \bar{\rho}_{\mathbf{q}}|\psi_0\rangle\,, \tag{27}$$

where $\bar{\rho}_{\mathbf{q}}$ is the *projected* density operator:[98]

$$\bar{\rho}_{\mathbf{q}} = \sum_{m,m'} \langle 0,m'|e^{-i\mathbf{q}\cdot\mathbf{r}}|0,m\rangle a^{\dagger}_{0,m'}a_{0,m} = \sum_{j=1}^{N} e^{-|q|^2/2}e^{-iq^* z_j/2}e^{-iq\frac{\partial}{\partial z_j}}\,, \tag{28}$$

where $|0,m\rangle$ correspond to single-particle states in the lowest LL and angular momentum m, $a^{\dagger}_{0,m}$ is the particle creator operator for such state, and we work in units of the magnetic length. The exclusion of inter-LL excitations eliminates the cyclotron mode. The excited states have a suggestive form:[98]

$$\bar{\rho}_{\mathbf{q}}\psi(z_1,\ldots,z_N) = \sum_{j=1}^{N} e^{-|q|^2/2}e^{-iq^* z_j/2}\psi(z_1,\ldots,z_{j-1},z_j - iq, z_{j+1},\ldots,z_N)\,, \tag{29}$$

which corresponds to shifting each electron by $\hat{e}_z \times \mathbf{q}$ and superimposing these N configurations with an amplitude $e^{-iq^* z_j/2}$. In a form analogous to Eq. (26), the excitation spectrum is given by

$$\bar{\Delta}_{\mathbf{q}} = \frac{(2N)^{-1}\langle\psi_0|[\bar{\rho}^{\dagger}_{\mathbf{q}},[\bar{H},\bar{\rho}_{\mathbf{q}}]]|\psi_0\rangle}{N^{-1}\langle\psi_0|\bar{\rho}^{\dagger}_{\mathbf{q}}\bar{\rho}_{\mathbf{q}}|\psi_0\rangle} \equiv \frac{\bar{f}(\mathbf{q})}{\bar{S}(\mathbf{q})}\,. \tag{30}$$

The projected oscillator strength comes from the non-commutation of the projected density operator with terms in the *potential* energy part of the Hamiltonian also projected onto the LLL:

$$\bar{H} = \frac{1}{2}\sum_{\mathbf{q}} v_{\mathbf{q}}(\bar{\rho}^{\dagger}_{\mathbf{q}}\bar{\rho}_{\mathbf{q}} - Ne^{-q^2/2})\,. \tag{31}$$

Since $[\bar{\rho}_{\mathbf{k}},\bar{\rho}_{\mathbf{q}}] = (e^{k^* q/2} - e^{kq^*/2})\bar{\rho}_{\mathbf{k}+\mathbf{q}}$, we find[78,79]

$$\bar{f}(\mathbf{q}) = 2e^{-|q|^2/2}\sum_{\mathbf{k}} \sin^2\left(\frac{\mathbf{q}\times\mathbf{k}}{2}\right)\bar{S}(\mathbf{k})[v_{\mathbf{k}-\mathbf{q}}e^{\mathbf{k}\cdot\mathbf{q}}e^{-|q|^2/2} - v_{\mathbf{k}}]\,. \tag{32}$$

For its part, the projected static structure factor $\bar{S}(\mathbf{q})$ can be calculated from:[78,79,98]

$$\bar{S}(\mathbf{q}) = S(\mathbf{q}) - (1 - e^{-q^2/2})\,. \tag{33}$$

For the quantum Hall liquid crystals, BRS states [Eq. (15)] corresponding to a $\nu = 1/3$ *nematic*, a $\nu = 1/5$ *tetratic*, and a $\nu = 1/7$ *hexatic* were considered. Figure 7 shows the pair correlation function for various states. In all cases, correlation functions and SMA excitation spectra were computed for numerous α-s. The angle dependence significantly increases the burden in the MC simulations since a high-quality, full angle-dependent $g(\mathbf{r})$ is needed, rather than the considerably simpler angle-averaged $g(r)$ for isotropic systems. The accurate calculation of $\bar{f}(\mathbf{q})$,

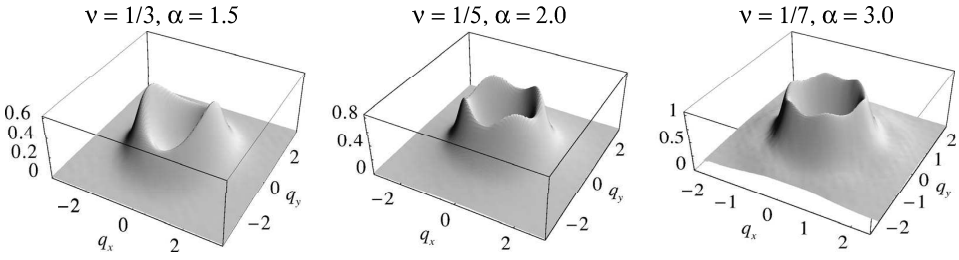

Fig. 14. *Projected* static structure factors $\bar{S}(\mathbf{q})$ for a $\nu = 1/3$ *nematic*, a $\nu = 1/5$ *tetratic*, and a $\nu = 1/7$ *hexatic*. In all cases, $\bar{S}(\mathbf{q}) = \mathcal{O}[q^4]$ for small q, and $\bar{S}(\infty) \to 0$.

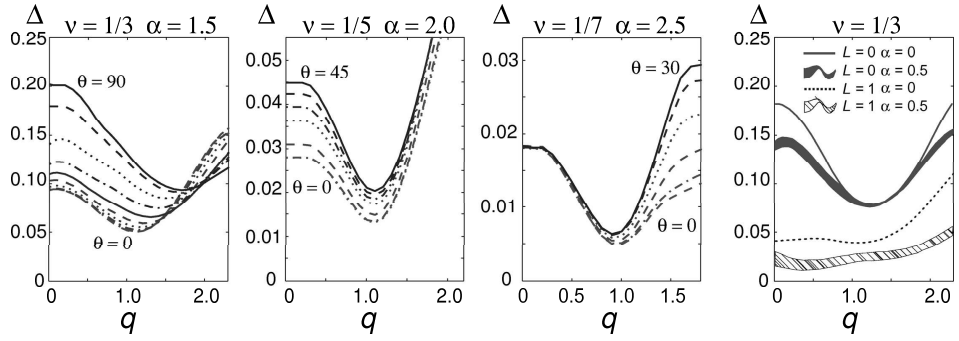

Fig. 15. Single mode approximation spectra for a $\nu = 1/3$ *nematic*, a $\nu = 1/5$ *tetratic*, and a $\nu = 1/7$ *hexatic*. Note the dramatic angular dependence of the spectra, and the appearance of a singular gap as $q \to 0$ for the nematic and tetratic. The rightmost panel shows also the spectrum for the $\nu = 1/3$ *nematic* in the first excited LL ($L = 1$).

with its angular-dependent exponentially large factors required high quality $\bar{S}(\mathbf{q})$ and hence $g(\mathbf{r})$. In our MC simulations for $g(\mathbf{r})$, we accumulated of the order of 10,000 counts in "boxes" of 0.01×0.01 (in units of l_0). Furthermore, a relatively large N_e is required so that the simulations are able to reproduce a system in the thermodynamic limit. The simulations, for each α and ν required ca. cpu×days of computation on a cluster of 2 GHz Athlon$^{\text{TM}}$ processors.[94,95]

Figure 14 shows the *projected* static structure factors $\bar{S}(\mathbf{q})$ for a $\nu = 1/3$ *nematic*, a $\nu = 1/5$ *tetratic* and a $\nu = 1/7$ *hexatic*. From $\bar{S}(\mathbf{q})$, the oscillator strength $\bar{f}(\mathbf{q})$ is computed using Eq. (32). Analysis of $\bar{S}(\mathbf{q})$ and $\bar{f}(\mathbf{q})$ shows that *both* are $\mathcal{O}[q^4]$ for small $\mathbf{q}$.[78,79]

Figure 15 presents the results for the excitation spectra in the lowest LL.[94,95] These are consistent with those obtained by GMP for the isotropic $\nu = 1/3$ and $1/5$ FQHE cases[78,79] which were qualitatively confirmed experimentally.[99,100] The SMA spectrum remains gaped, with a deep magnetoroton. BRS states have significant anisotropy in their spectra, and most noteworthy is the fact that for the nematic and tetratic cases the spectrum is *singular*, with an angle dependence on the excitation energy $\Delta(\mathbf{q})$ as $\mathbf{q} \to 0$ (the hexatic has a regular spectrum). The apparent disparity

have, of course, to do with the different rotational symmetries of the different states: as $\bar{\Delta} = \bar{f}/\bar{S}$, and both numerator and denominator are $\mathcal{O}[q^4]$ for small $\mathbf{q}$, there is no possibility of generating a C_6 symmetric form with terms that can only depend on q_x^4, q_y^4, and $q_x^2 q_y^2$. This can also be understood from the point of view of an effective elasticity theory for 2DES (valid in the long wavelength limit, $q \to 0$):[101] the elasticity tensor being of the fourth rank is not compatible with a six-fold rotational symmetry.[102]

The presence of this singular spectrum suggests that microwave conductivity experiments[99,100,103] may be able to discern such structures as a signature of, e.g. the quantum Hall nematic suggested by magnetotransport experiments.[32–35,36,104]

Theoretical predictions of which type of order is lowest in *free* energy (required to decide which state is favorable at *finite temperatures*, as shown in Refs. 15 and 104) are still incomplete, however, as the entropy is likely to be dominated by gapless modes originating, e.g. from the Goldstone modes associated with the spontaneous breaking of the continuous rotational symmetry of the isotropic states. Generalization of the SMA to gapless rotational modes (see e.g. Ref. 62–64) will require, however, three-body operators which demanding considerably higher computing capabilities.[105]

7. Conclusions

In the earlier part of this paper we showed that "melted" CDW-s (i.e. the nematics derived from the smectic via the Landau–Peierls argument) are obvious candidates to explain the onset of anisotropy on clean 2DES when electrons occupy the excited Landau levels. These ideas successfully produced anisotropic-isotropic transition temperatures in semi-quantitative agreement with experiments (Sec. 4). In essence, the onset of anisotropy does not signal the *emergence* of charge-density modulation, but reflects the *orientational ordering* of electronic domains with some pre-existing small-scale charge-density modulation.

Since the underlying smectic is known to be melted at any finite temperature, it is natural to question whether it is necessary at all, i.e. whether it is possible to establish states with appropriate broken rotational symmetries at the quantum level. In other words, whether there is a reasonable microscopic theory for (anisotropic) quantum Hall liquid crystalline states with no positional or translational order. In Sec. 5 we showed precisely that it is possible to construct such states, which need to satisfy the following conditions:

(i) the states must obey Fermi statistics;
(ii) the states must be translationally invariant (at least far away from the boundaries when small finite systems are considered);
(iii) there must be a broken rotational symmetry belonging to the proper symmetry group; and
(iv) the states must belong to a single LL.

The states proposed for (i) Laughlin-like states, $\nu = 2L + 1/m$ where $L = 0, 1, \ldots$ and $m = 3, 5, 7$; and (ii) half-filled RR-like states, $\nu = 2L + 1/2$ where $L = 0, 1, \ldots$; were build from the standard isotropic states by by systematically splitting the degenerate zeros of the wavefunctions (or alternatively, by moving the vortices of the composite fermions away from the electrons themselves).

In such a way, anisotropy is inherently built into the wave function. The anisotropy parameters, α_μ, introduce a preferred set of directions into the wave function thus creating a degree of anisotropy. They are distributed in pairs of opposite value in the complex plane (to satisfy Fermi statistics). For simplicity we consider states with the highest level of discrete symmetry possible at each filling factor, set by distributing the α_μ symmetrically in a circle around the origin. For the LLL ($L = 0$) and first excited LL ($L = 1$) the splitting of the zeros is energetically favorable, but in the next LL ($L = 2$) the splitting reduces the correlation energy, making the BRS liquid crystalline states favorable. These results indicate that there is a concrete possibility and promise that a BRS liquid crystalline phase could explain the large magnetotransport anisotropy observed at high Landau levels with index $L \geq 2$.

In the latter part of this paper, we showed how the spectrum of excitations of these liquid crystalline states may be computed in the single mode approximation, a reliable method that yields the first moment (average) of all excitation energies of modes that have a non-zero overlap of the density operator with the ground state, thus making these types of modes easier to experimentally probe electromagnetically. Characterization of the BRS states using microwave conductance experiments is suggested.

Acknowledgments

We would like to thank A. T. Dorsey, A. H. MacDonald, S. Girvin, E. Fradkin, H. Fertig, M. Fogler, G. Vignale, C. M. Lapilli and J. Jain for useful discussions. Acknowledgment is made to the University of Missouri Research Board and Research Council, and to the Donors of the Petroleum Research Fund, administered by the American Chemical Society, for support of this research. Orion Ciftja would like to acknowledge support by the U.S. D.O.E. (Grant No. DE-FG52-05NA27036).

References

1. K. von Klitzing, G. Dorda and M. Pepper, *Phys. Rev. Lett.* **45**, 494 (1980).
2. D. C. Tsui, H. L. Stormer and A. C. Gossard, *Phys. Rev. Lett.* **48**, 1559 (1982).
3. R. B. Laughlin, *Phys. Rev. Lett.* **50**, 1395 (1983).
4. S. Das Sarma and A. Pinczuk (eds.), *Perspectives in Quantum Hall Effects* (John Wiley, New York, 1996).
5. R. E. Prange and S. M. Girvin (eds.), *The Quantum Hall Effect*, 2nd edn. (Springer-Verlag, New York, 1990).
6. D. J. Thouless, *Topological Quantum Numbers in Nonrelativistic Physics* (World Scientific, Singapore, 1998).

7. X. G. Wen, *Phys. Rev. B* **43**, 11 025 (1991).
8. X. G. Wen, *Phys. Rev. Lett.* **64**, 2206 (1990).
9. J. K. Jain, *Phys. Rev. Lett.* **63**, 199 (1989).
10. P. K. Lam and S. M. Girvin, *Phys. Rev. B* **30**, R473 (1984).
11. K. Esfarjani and S. T. Chui, *Phys. Rev. B* **42**, 10 758 (1990).
12. X. Zhu and S. G. Louie, *Phys. Rev. Lett.* **70**, 335 (1993).
13. X. Zhu and S. G. Louie, *Phys. Rev. B* **52**, 5863 (1995).
14. K. Yang, F. D. M. Haldane and E. H. Rezayi, *Phys. Rev. B* **64**, 081 301 (2001).
15. W. Pan, H. L. Stormer, D. C. Tsui, L. N. Pfeiffer, K. W. Baldwin and K. W. West, *Phys. Rev. Lett.* **88**, 176 802 (2002).
16. R. L. Willett, M. A. Paalanen, R. R. Ruel, K. W. West, L. N. Pfeiffer and D. J. Bishop, *Phys. Rev. Lett.* **65**, 112 (1990).
17. R. L. Willett, R. R. Ruel, M. A. Paalanen, K. W. West and L. N. Pfeiffer, *Phys. Rev. B* **47**, 7344 (1993).
18. R. L. Willett, R. R. Ruel, K. W. West and L. N. Pfeiffer, *Phys. Rev. Lett.* **71**, 3846 (1993).
19. B. I. Halperin, P. A. Lee and N. Read, *Phys. Rev. B* **47**, 7312 (1993).
20. R. L. Willett, J. P. Eisenstein, H. L. Stormer, D. C. Tsui, A. C. Gossard and J. H. English, *Phys. Rev. Lett.* **59**, 1779 (1987).
21. W. Pan, J.-S. Xia, V. Shvarts, D. E. Adams, H. L. Stormer, D. C. Tsui, L. N. Pfeiffer, K. W. Baldwin and K. W. West *Phys. Rev. Lett.* **83**, 3530 (1999).
22. F. D. M. Haldane and E. Rezayi, *Phys. Rev. Lett.* **60**, 956 (1988) [Erratum *ibid.* **60**, 1886 (1988)].
23. A. H. Mac Donald, D. Yoshioka and S. M. Girvin, *Phys. Rev. B* **38**, 3636 (1988).
24. R. Morf and N. d'Ambrumenil, *Phys. Rev. Lett.* **74**, 5116 (1995).
25. G. Moore and N. Read, *Nuclear Physics B* **360**, 362 (1991).
26. V. W. Scarola, K. Park and J. K. Jain, *Nature* **406**, 863 (2000).
27. N. Read and D. Green, *Phys. Rev. B* **61**, 10 267 (2000).
28. N. Read, *Physica B* **298**, 121 (2001).
29. A. A. Koulakov, M. M. Fogler and B. I. Shklovskii, *Phys. Rev. Lett.* **76**, 499 (1996).
30. M. M. Fogler, A. A. Koulakov and B. I. Shklovskii, *Phys. Rev. B* **54**, 1853 (1996).
31. R. Moessner and J. T. Chalker, *Phys. Rev. B* **54**, 5006 (1996).
32. M. P. Lilly, K. B. Cooper, J. P. Eisenstein, L. N. Pfeiffer and K. W. West, *Phys. Rev. Lett.* **82**, 394 (1999).
33. R. R. Du, D. C. Tsui, H. L. Stormer, L. N. Pfeiffer, K. W. Baldwin and K. W. West, *Solid State Comm.* **109**, 389 (1999).
34. M. Shayegan, H. C. Manoharan, S. J. Papadakis and E. P. DePoortere, *Physica E* **6**, 40 (2000).
35. J. P. Eisenstein, M. P. Lilly, K. B. Cooper, L. N. Pfeiffer and K. W. West, *Physica E* **9**, 1 (2001).
36. K. B. Cooper, M. P. Lilly, J. P. Eisenstein, L. N. Pfeiffer and K. W. West, *Phys. Rev. B* **65**, 241 313(R) (2002).
37. K. B. Cooper, M. P. Lilly, J. P. Eisenstein, L. N. Pfeiffer and K. W. West, *Phys. Rev. B* **60**, 11285 (1999).
38. J. P. Eisenstein, M. P. Lilly, K. B. Cooper, L. N. Pfeiffer and K. W. West, *Physica A* **6**, 29 (2000).
39. J. P. Eisenstein, K. B. Cooper, L. N. Pfeiffer and K. W. West, *Phys. Rev. Lett.* **88**, 076 801 (2002).
40. E. E. Mendez, M. Heilblum, L. L. Chang and L. Esaki, *Phys. Rev. B* **28**, 4886 (1983).
41. V. J. Goldman, M. Shayegan and D. C. Tsui, *Phys. Rev. Lett.* **61**, 881 (1988).

42. J. R. Mallett, R. G. Clark, R. J. Nicholas, R. L. Willett, J. J. Harris and C. T. Foxon, *Phys. Rev. B* **38**, 2200 (1988).
43. R. Price, X. Zhu, P. M. Platzman and S. G. Louie, *Phys. Rev. B* **48**, 11 473 (1993).
44. P. M. Platzman and R. Price, *Phys. Rev. Lett.* **70**, 3487 (1993).
45. E. Fradkin and S. A. Kivelson, *Phys. Rev. B* **59**, 8065 (1999).
46. S. A. Kivelson, E. Fradkin and V. J. Emery, *Nature (London)* **393**, 550 (1998).
47. C. Wexler and A. T. Dorsey, *Phys. Rev. B* **64**, 115 312 (2001).
48. E. Fradkin, S. A. Kivelson, E. Manousakis and K. Nho, *Phys. Rev. Lett.* **84**, 1982 (2000).
49. J. Toner and D. R. Nelson, *Phys. Rev. B* **23**, 316 (1981).
50. J. M. Kosterlitz and D. J. Thouless, *J. Phys. C* **6**, 1181 (1973).
51. J. M. Kosterlitz, *J. Phys. C* **7**, 1046 (1974).
52. V. L. Berezinsky, *ZETP* **59**, 907 (1970).
53. V. L. Berezinsky, *ZETP* **61**, 1144 (1971).
54. A. H. MacDonald, *Phys. Rev. B* **30**, 4392, (1984).
55. T. Jungwirth *et al.*, *Phys. Rev. B* **60**, 15 574, (1999).
56. T. D. Stanescu, I. Martin and P. Phillips, *Phys. Rev. Lett.* **84**, 1288 (2000).
57. A. Manolescu and R. R. Gerhardts, *Phys. Rev. B* **56**, 9707 (1997).
58. A. H. MacDonald and S. M. Girvin, *Phys. Rev. B* **38**, 6295 (1988).
59. D. R. Nelson and R. A. Pelcovits, *Phys. Rev. B* **16**, 2191 (1977).
60. V. Oganesyan, S. A. Kivelson and E. Fradkin, *Phys. Rev. B* **64**, 195 109 (2001).
61. H. Y. Kee, *Phys. Rev. B* **67**, 073 105 (2003).
62. L. Radzihovsky and A. T. Dorsey, *Phys. Rev. Lett.* **88**, 216 802 (2002).
63. M. M. Fogler and V. M. Vinokur, *Phys. Rev. Lett.* **84**, 5828 (2000).
64. M. M. Fogler, *Europhys. Lett.* **66**, 572 (2004).
65. B. I. Halperin and D. R. Nelson, *Phys. Rev. Lett.* **41**, 121 (1978).
66. A. P. Young, *Phys. Rev. B* **19**, 1855 (1979).
67. K. Musaelian and R. Joynt, *J. Phys.: Condens. Matter* **8**, L105 (1996).
68. L. Balents, *Europhys. Lett.* **33**, 291 (1996).
69. O. Ciftja and C. Wexler, *Phys. Rev. B* **65**, 045 306 (2002).
70. C. Wexler and O. Ciftja, *J. Phys.: Condens. Matter* **14**, 3705 (2002).
71. A. J. Schmidt, O. Ciftja and C. Wexler, *Phys. Rev. B* **67**, 155 315 (2003).
72. O. Ciftja, C. M. Lapilli and C. Wexler, *Phys. Rev. B* **69**, 125 320 (2004).
73. F. C. Zhang and S. Das Sarma, *Phys. Rev. B* **33**, 2903 (1986).
74. R. Morf and B. I. Halperin, *Phys. Rev. B* **33**, 2221 (1986).
75. O. Ciftja and C. Wexler, *Phys. Rev. B* **67**, 075 304 (2003).
76. N. Metropolis, A. W. Rosenbluth, M. N. Rosenbluth, A. M. Teller and E. Teller, *J. Chem. Phys.* **21**, 1087 (1953).
77. S. He, F. C. Zhang, X. C. Xie and S. Das Sarma, *Phys. Rev. B* **42**, 11 376 (1990).
78. S. M. Girvin, A. H. MacDonald and P. M. Platzman, *Phys. Rev. Lett.* **54**, 581 (1985).
79. S. M. Girvin, A. H. MacDonald and P. M. Platzman, *Phys. Rev. B* **33**, 2481 (1986).
80. E. Rezayi and N. Read, *Phys. Rev. Lett.* **72**, 900 (1994).
81. O. Ciftja and C. Wexler, *Phys. Rev. B* **65**, 205 307 (2002).
82. S. Fantoni and S. Rosati, *Nuovo Cim. Lett.* **10**, 545 (1974).
83. S. Fantoni and S. Rosati, *Nuovo Cim. A* **25**, 593 (1975).
84. E. Krotscheck and M. L. Ristig, *Phys. Lett. A* **48**, 17 (1974).
85. E. Krotscheck and M. L. Ristig, *Nucl. Phys. A* **242**, 389 (1975).
86. J. G. Zabolitzky, *Phys. Rev. A* **16**, 1258 (1977).
87. E. Manousakis, S. Fantoni, V. R. Pandharipande and Q. N. Usmani, *Phys. Rev. B* **28**, 3770 (1983).

88. M. L. Ristig and J. W. Clark, *Phys. Rev. B* **14**, 2875 (1976).
89. O. Ciftja and S. Fantoni, *Phys. Rev. B* **56**, 13 290 (1997).
90. G. Ripka, *Physics Reports* **56**, 1 (1979).
91. N. Trivedi and J. K. Jain, *Mod. Phys. Lett. B* **5**, 503 (1993).
92. R. P. Feynman, *Phys. Rev.* **91**, 1291 (1953).
93. R. P. Feynman, *Phys. Rev.* **94**, 262 (1954).
94. C. M. Lapilli and C. Wexler, *AIP Conf. Proc.* **772**, 543 (2005).
95. C. M. Lapilli and C. Wexler, *Phys. Rev. B* (2006, in press), preprint cond-mat/0506740.
96. K. Park and J. K. Jain, *Solid State Comm.* **115**, 353 (2000).
97. W. Kohn, *Phys. Rev.* **123**, 1242 (1961).
98. S. M. Girvin, *Phys. Rev. B* **30**, 558 (1984).
99. A. Pinczuk, B. S. Dennis, L. N. Pfeiffer and K. West, *Phys. Rev. Lett.* **70**, 3983 (1993)
100. A. Pinczuk, B. S. Dennis, L. N. Pfeiffer and K. West, *Physica B* **249**, 40 (1998).
101. S. Conti and G. Vignale, *J. Cond. Mat. Phys.* **10**, L779 (1998).
102. C. M. Lapilli, C. Wexler and G. Vignale, *Bull. Am. Phys. Soc. II* **50**(1), 1272 (2005), paper in preparation.
103. R. M. Lewis, Y. Chen, L. W. Engel, D. C. Tsui, P. D. Ye, L. N. Pfeiffer, and K. W. West *Phys. Rev. Lett.* **93**, 176 808 (2004).
104. G. Gervais, L. W. Engel, H. L. Stormer, D. C. Tsui, K. W. Baldwin, K. W. West and L. N. Pfeiffer, *Phys. Rev. Lett.* **93**, 266 804 (2004).
105. M. M. Fogler, private communication.